Development of Protein-targeted Aptamers for Cancer Therapeutics

Yunshi Zhou

A thesis

submitted in partial fulfillment of the

requirements for the degree of

Master of Science

University of Washington

2020

Committee:

Suzie H. Pun

Patrick S. Stayton

Program Authorized to Offer Degree:

Bioengineering

University of Washington

Abstract

Development of Protein-targeted Aptamers for Cancer Therapeutics

Yunshi Zhou

Chair of the Supervisory Committee:
Robert F. Rushmer Professor Suzie H. Pun
Bioengineering

Aptamers are single-stranded DNA or RNA molecules capable of recognizing and tightly binding to a variety of targets with high specificity. Treatment of brain and CNS disorders remains the holy grail of drug delivery due to the obstacle imposed by the blood-brain barrier (BBB). Bearing various advantages such as small size, low immunogenicity, and ease of large-scale synthesis at affordable costs, aptamers are an emerging field of novel cancer therapeutics that demonstrate the potential for BBB crossing. Here, we aimed to develop aptamer-based targeting vehicles utilizing the endogenous iron-loading pathway involving the transferrin receptor (TfR, or CD71) and its ligand, transferrin (Tf). We demonstrated our expansive effort in the discovery of Tf binding aptamers via protein-SELEX (**Chapter 2**) and the characterization, cross-reactivity, and preliminary data for future applications of a CD71 binding aptamer, tJBA (**Chapter 3**).

TABLE OF CONTENTS

LIST OF FIGURES

LIST OF TABLES

ACKNOWLEDGEMENTS

I am profoundly grateful to be surrounded by an amazing team of mentors, labmates, and friends in graduate school. This work would not be possible without all your support in the past two years. From a rookie undergraduate to a rookie scientist and engineer, I am so glad that my journey at UW Bioengineering had your company.

I would like to express my sincere gratitude to my thesis advisor **Prof. Suzie Pun**, for your guidance and insights in my research work as well as your tremendous support in helping me to start my career as a bioengineer. Thank you for giving me the opportunity to join your lab. No words could express how thankful I am to be part of the Punion family. You are the coolest scientist I have ever met and the role model I look to for the better of myself.

I would also like to express my deepest gratitude to my mentor **Nataly Kacherovsky**, for your most patient guidance and cheerful enthusiasm for science. You taught me how to conduct every single one of the experiments in the Pun lab; You lay the groundwork of every project I worked in and deserve all the credits of this work. Thank you for introducing me to the world of aptamers, teaching me that there is always a solution, and always pushing the boundary of my knowledge and research capability.

To my "Aptamer-mates" **Ian Cardle** and **Emmeline Cheng**, for always offering tremendous guidance and help with my projects and experiments. You are experts on aptamers and the immediate people I turn to for help. I extremely appreciate your patience in answering all my weird or stupid questions at any time, for sitting down with me and generously offering suggestions and advice for my research.

To **Dr. Drew Sellers**, for being the most helpful and most cheerful labmate/mentor I have ever worked with. Thank you for making me realize that I should always feel confident and proud of my work, for helping me set up the connection to the printer the very first day I joined Pun Lab, and for leaving Twizzlers on my desk. I feel honored to share the same enthusiasm as you about coffee.

To all the Pun lab members, both present and past: **Meilyn Sylvestre**, for your help with the plate reader, animal work, and always triggering a fun conversation; **Albert Yen**, for teaching me how to harvest a spleen for single-cell suspension; **Audrey Olshefsky**, for your tremendous help with Rosetta; **Marti Tooley**, for teaching me how to perform capillary electrophoresis; **Alex Prossnitz**, for your critical insight during group meetings, which later turned out to be the key issue of my project design; **Dr. Daniel Lee**, for telling me not to feel nervous but to enjoy the final exam; **Dr. Bob Lamm**, for extremely useful tips on oral presentation; **Lucy Yang**, for being an expert on how to manipulate Autoclave and introducing your fish tank; **Clinton Heinze**, **Trey Pichon**, **Dr. Gary Liu**, **Dr. David Peeler**, and **Dr. Shixian Lyu**, for all the help, support, and friendship.

To my committee member **Prof. Pat Stayton**, for teaching me how to think as an advanced molecular biologist and engineer. Your lectures and knowledge provided me with so much insight into my projects and challenged me to grow as a critical thinker. “Hydrophobic interactions!”

To my undergraduate research mentor **Prof. Wei Chen**, thank you for your support and kindness all the way from the very first day I joined your lab. You taught me to how to research and to think as a researcher from Ground Zero.

To my fellow bioengineers and friends, **Rongyu Zhang**, **Joyce Lu**, **Henry Lee**, and **Sijia Li**. I am incredibly fortunate to meet such great friends in Seattle. I will forever remember those days when we hunted after seats in the library, enjoyed crepes after a presentation, and held hot pot parties.

To all my friends from the dance group **the KOMPANY**, for taking my mind off lab and experiments for a short moment, for making me feel belonged and welcomed at UW, and for our fun time dancing together at the IMA and on stage.

To my family and dearest friends, **Sissi Shen**, **Nina Zhou**, **Shen Ren**, **Yifei Ren**, and **Tianye Yang**, for welcoming me with open arms when I first arrived in Seattle. I could not imagine how my life would be without your company. Can’t wait to share shaved ice and taro balls with you at MeetFresh!

To my boyfriend **Kaisheng Song**, for joining my life, standing by my side, and cheering for all my progress in the past five years. Thank you for always offering a shoulder to cry on and motivating me to be my better self.

To my parents, **Hanjiang Ma** and **Zhenxing Zhou**, for your unconditional love and biggest support. I will forever be grateful for letting me have the opportunity to pursue my interests and passions. You taught me how to love, respect, and cherish. You have helped shape the person I have become and I could not ask for better parents.

Chapter 1. INTRODUCTION

Abstract

Aptamers are single-stranded DNA or RNA targeting molecules possess binding affinities comparable to or even higher than those of antibodies. They are discovered through a library selection method named systematic evolution of ligands by exponential enrichment (SELEX). The blood-brain barrier (BBB) remains a tremendous obstacle for the delivery of drugs to treat brain diseases. One promising strategy to overcome the BBB is to target the endogenous receptor-mediated transport (RMT) systems on the BBB endothelium. Being small, non-immunogenic, storage stable, and easy-to-make, aptamers are ideal candidates for this purpose. We introduce recent improvements on the stability of aptamers and the efficiency of SELEX to push the aptamer field towards translational research. In particular, we focus on the potential of aptamers as targeting molecules to gain improved access to the brain via RMT.

1.1 INTRODUCTION TO APTAMERS

Aptamers are short single-stranded (ss) nucleic acid sequences, synthetically made to be capable of binding to targets with high affinity and specificity. First introduced simultaneously by two groups in 1990, the term “aptamer” originates from the Latin word "aptus" which means “fit”, and the Greek suffix "-meros", which means “portion”.[1,2] Merging as a new class of ligands, aptamers can bind to various targets, including ions, small molecules, peptides, proteins, viruses, living cells and whole microorganisms.[3] Aptamers are developed via an *in vitro* Darwin screening technique known as Systematic Evolution of Ligands by Exponential enrichment (SELEX), which selects for sequences of interest under specific conditions from a nucleic acid library containing 10^{13} to 10^{15} unique sequences.[2] Aptamers can be utilized for target function modulation, cargo delivery,

or be used in diagnostic and analytical assays.[4] Applications of aptamers span wide from clinical diagnostics and therapeutic agents to food safety inspection and environment monitoring.[3] Compared to antibodies, which are usually considered their functional counterparts, aptamers possess advantages including easy synthesis process, prolonged shelf life, broad targeting objects, and lower to no immunogenicity.[5]

1.1.1 *Properties of Aptamers*

1.1.1.1 Structure, affinity, specificity, stability, and modification

Affinity and specificity are two critical parameters of any targeting molecules to determine its efficiency. The two characteristics lay the foundation for developing drug delivery systems for therapeutic applications. Aptamers are constructed of ss nucleic acid sequences. They are thus capable of folding into a variety of complex 3D structures (**Figure 1.1**) produced by a combination of Watson-Crick base pairing and non-canonical inter-molecular interactions.[6] The sophisticated recognition properties as well as the capability to bind tightly and specifically originates from the shape complementarity and non-covalent interactions, such as Van der Waals force, hydrogen bonding, and stacking interactions.[7] The binding affinities are usually quantified by the equilibrium dissociation constants (K_d), which are often within a low nanomolar range, comparable to those of antibodies.[7] Approximately 80% of the first 100 aptamers selected by NeXstar/Gilead Sciences had K_d values less than 1 nM.[8] The results are even more prominent considering the fact that the comparison is usually made between a monovalent aptamer and a divalent antibody.

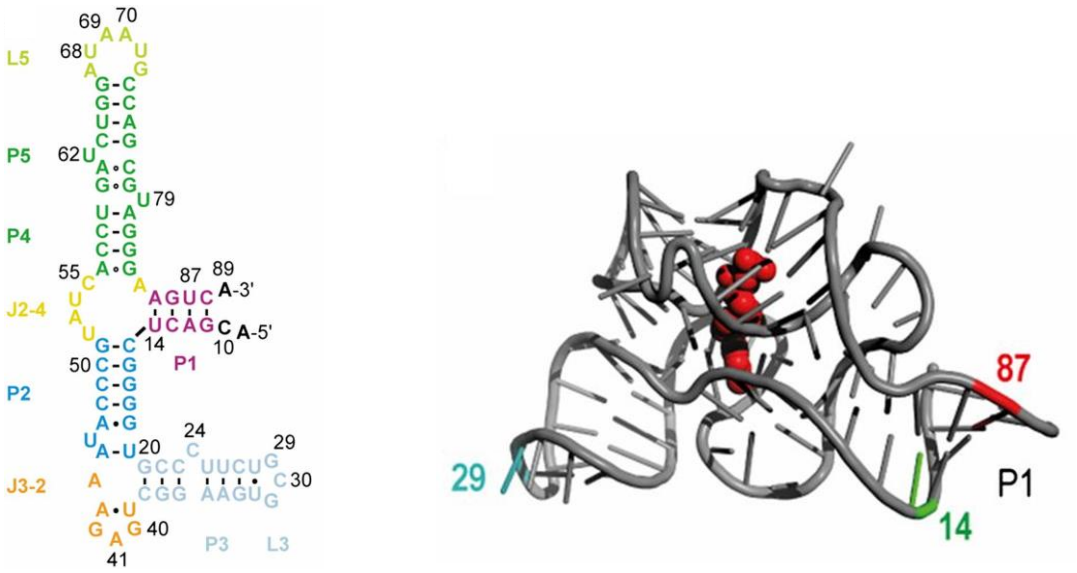

Figure 1.1 Secondary and 3D structure of aptamers.
An example of the secondary structure representation of a Thiamine pyrophosphate (TPP) riboswitch aptamer (left) and its 3D structure representation of aptamer/TPP complex(right).[9]

Due to the nature of nucleic acids, unmodified aptamers have limited stability *in vivo*. The folding of aptamers is sensitive to temperature change, as an increase in temperature might disrupt the tertiary structure that enables binding ability as well as accelerate their degradation by nucleases. Unmodified nucleic acids last less than 5 min in serum, and are rapidly hydrolyzed by endo- and exonucleases.[10] As a result, various chemical modifications have been applied to the nucleotides to improve their stability *in vivo* for clinical applications.[11] Modifications can be incorporated into aptamers after the SELEX or during the SELEX protocol. The location of the modification can be at the sugar, base, and/or phosphate backbone.

The most common post-SELEX modifications on the sugar ring is implemented at 2'-position of the (deoxy-)ribose sugar unit (**Figure 1.2 A-C**). Due to the fact that Ribonuclease A (RNase A) targets the 2′-hydroxyl group and breaks the phosphodiester bond, replacing the 2′-hydroxyl group improves the stability of nucleic acids.[12] For instance, pegaptanib (Macugen), the only FDA-approved oligonucleotide-based drug on the market, is composed of 2′-fluoro(2′-F) pyrimidine N*TPs and 2′-methoxy(2'Ome) purine N*TPs.[13] 2′-deoxy-2′-fluoro-β-D-arabinose

(FANA) represents another 2′-modification that improves thermal stabilization and the resistance against nuclease degradation (**Figure 1.2 D**).[14,15] The sugar ring was locked in a 2′-endo "south" pucker formation, which were also found to improve their affinities for both complementary DNA and RNA sequences.[15] Lock nucleic acid (LNA) is a common strategy for stabilizing the sugar ring structure (**Figure 1.2 E**). In LNAs, the C3′-endo conformation of sugar is enforced by a methylene linker connecting the O2′ to the C4′ position,[16,17] which significantly increases the thermal stability.

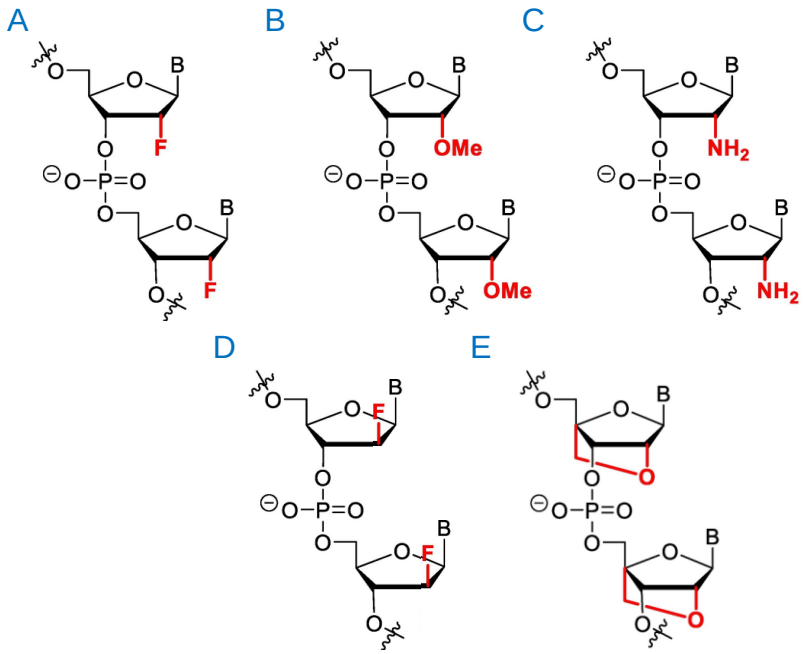

Figure 1.2 Chemical structures of modifications at the sugar ring.[18]
Modifications at C-2 position to improve nuclease resistance and thermal stability of aptamers: (A) 2′-fluoro-RNA (2′-F); (B) 2′-methoxy-RNA (2′-OMe); (C) 2′-amino-RNA (2′-NH2); (D) 2′-deoxy-2′-fluoro-β-D-arabinose (FANA); (E) Lock nucleic acid (LNA).

Chemical modifications can also be incorporated into aptamers during the SELEX protocol, since post-SELEX modifications increase the risk of adding conformational changes to the aptamer that it loses its binding affinity.[19] Aptamers obtained with modifications during SELEX can also be further functionalized by post-SELEX strategies. The purpose, besides enhancing stability and improving renal clearance, is to circumvent the intrinsic diversity constraints of

natural nucleotides and to greatly expand the chemical diversity of aptamers so that the range of accessible protein targets is broadened. The main binding contributors of natural nucleotides - A, T, C, G, U, to targets are van der Waals, hydrogen bonding, and electrostatic interactions.[6] Compared to antibody-ligand binding, in which hydrophobic interactions play a critical role in making the entire binding reaction favorable,[20] aptamer binding mainly relies on these polar interactions. Modified nucleotides can introduce increased contact interactions, such as hydrophobic interactions, with their intended targets as well as novel secondary and tertiary folds and structures. Different modifications can usually be achieved via modulating enzymatic polymerization during SELEX. The wide variety of modifications include but not limited to protein-like residues,[21] carborane,[22] oligonucleotides,[23] and enzymes.[24]

Slow Off-rate Modified Aptamers (SOMAmers) are among the most common base modifications.[25] Nucleotide triphosphate analogs modified at the 5-position (R) of dUTP and/or at the dCTP (**Figure 1.3**) are incorporated in SELEX.[26] The added protein-like properties of bases create hydrophobic surfaces on aptamers that can interact with hydrophobic regions of amino acids on the protein targets. The added hydrophobic interactions significantly lowers the off rate and greatly improves the binding affinity of the aptamers.[25]

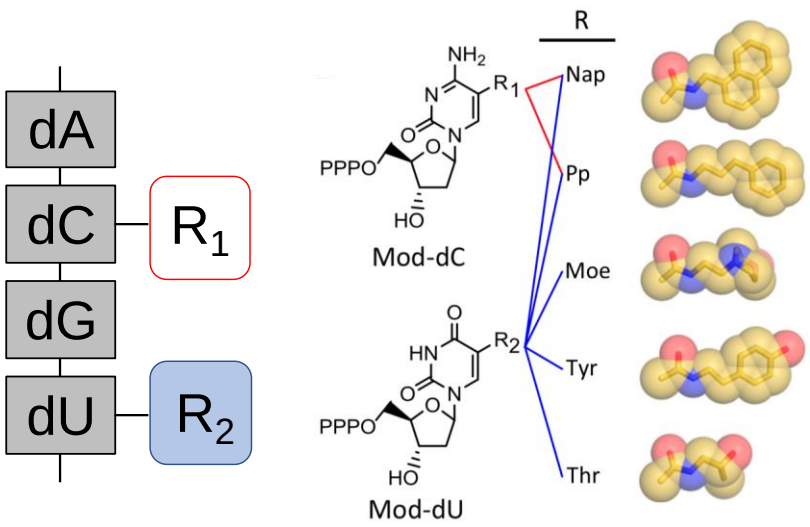

Figure 1.3 Schematics and chemical structures of base modifications.
Modified nucleotides at 5-position (R) of cytidine and uridine: Nap, 5-[N-(1-naphthylmethyl) carboxamide]-2′-deoxy; Pp, 5-[N-(phenyl-3-propyl)carboxamide]-2′-deoxy; Moe, 5-[N-(1-morpholino-2-ethyl)carboxamide]-2′-deoxy; Tyr, 5-[N-(4-hydroxyphenyl-2-ethyl)carboxamide]-2′-deoxy; and Thr, 5-[N-(S-2-hydroxypropyl)carboxamide]-2′-deoxy.[26]

Modifications targeting phosphate backbones can also be implemented during SELEX, though less common compared to base modifications. The phosphodiester linkage can be replaced with non-bridging phosphate oxygens by Sulphur (**Figure 1.4 A**).[27] An example is the increased affinity and improved nuclease resistance in an RNA aptamer selected for binding of thrombin.[28] The favorable interaction between the sulfur and the phenylalanine residues of the thrombin target contributes to an improved affinity from 1871 pM to 1.8 pM.[28] Other interesting strategies to improve stability of aptamers include a new type of oligonucleotides called Spiegelmers (**Figure 1.4 B**). Spiegelmers are aptamers composed of L- rather than D-DNA and RNA scaffolds of the original nucleic acids, making them unrecognizable to nucleases.[29] Both strategies provide significant resistance to enzyme degradation.[30]

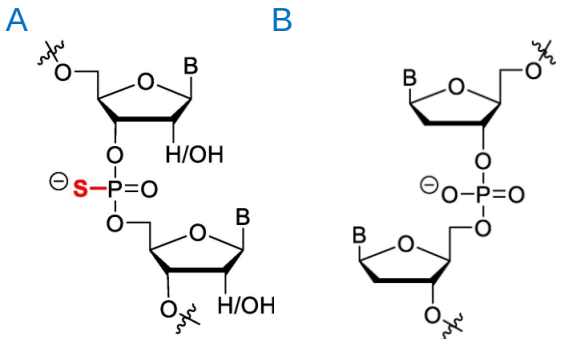

Figure 1.4 Chemical structures of backbone modifications (A) and Spiegelmers (B).[18]
The phosphodiester linkage of oligonucleotides is replaced with non-bridging phosphate oxygens by Sulphur. Spiegelmers are composed of L- rather than D-DNA/RNA scaffolds.

1.1.1.2 Size, tissue penetration, and renal filtration

Aptamers are typically 80 to 110 nucleotides (nt) long, consisting of a random region flanked by two fixed regions. The average masses of aptamers are between 6 - 30 kDa, 5 - 20 times smaller than antibodies. Due to their small size, aptamers usually experience high renal clearance, as the kidney filters out any compounds smaller than 40kDa in size.[31] A common solution is the conjugation of bulky complexes, including polyethylene glycol (PEG),[32] cholesterol,[33] and multimeric aptamers[32] to improve bioavailability of aptamers in the blood circulation. One study has shown that a cholesterol conjugated aptamer (chol-aptamer) efficiently entered the cell and implemented targeting functions without causing any abnormalities in mice.[33] Cholesterol conjugation showed dose proportionality, extended plasma circulation time, and enhanced aptamer bioavailability.[33]

On the other hand, the smaller size of aptamers compared to antibodies also offer faster tissue penetration, rapid cell internalization, and longer retention in tissues.[34,35] The aforementioned features are critical for therapeutic agents in a successful cancer treatment. Insufficient penetration into cancerous tissues will lead to low drug bioavailability, increased drug resistance and failure of tumor reduction.[36] One study has shown that a PEGylated EpCAM aptamer has a 4.3-fold longer sustained signal than that of the EpCAM antibody in mouse

colorectal cancer xenograft model.[34] At 200 μm distances from the blood vessels, the aptamer also performed 4-fold better tumor penetration in xenograft tumors than that of the antibody, detected 3 h after intravenous injection.[34]

1.1.1.3 Toxicity and immunogenicity

One of the most prominent features of aptamers is their low toxicity and low immunogenicity *in vivo*.[19] However, there are studies suggesting that chemical modifications could potentially cause some level of toxicity, inflammatory response and side effects.[37] For instance, studies have shown that LNA aptamers induce a hepatotoxic effect due to accumulation in the liver,[38] and phosphorothioate linkage modification may induce nonspecific interactions.[27] Some parts of the synthetic aptamers might be recognized by pattern recognition receptors (PRR) of the immune system and provoke an immune response. Study has shown that 2′-F-RNA stimulates toll-like receptors 3 and 7, leading to increased cell death and interferon-β expression in human cancer cells compared to unmodified RNAs.[39] Therefore, depending on the therapeutic applications, the ability of aptamers to activate or limit immunogenicity should be closely controlled.[39] Sufficient pre-clinical studies should be carried out to evaluate the toxicity and immunogenicity of aptamers before going into clinical evaluation.

1.1.2 *Production of Aptamers - SELEX*

Aptamers are usually generated by an *in vitro* iterative selecting methodology called Systematic Evolution of Ligands by Exponential enrichment (SELEX) (**Figure 1.5**). The main workflow of SELEX can be summarized in 3 steps: (1) Incubation: the target of interest is first incubated with a pool of aptamers with random sequences. The initial library typically contains at least 10^{14} unique reads. (2) Separation: after incubation, the unbound sequences are washed away, while bound sequences are eluted from the target and purified. (3) Amplification: the bound sequences are then

enriched to become the pool for the next round of SELEX. The stringency of SELEX can be altered by controlling physicochemical parameters such as concentration, pH, temperature, or buffer composition. Typically, after 5 - 15 rounds, aptamers with high affinity and specificity become the most represented in the pool. The pool sequence is subjected to Next Generation Sequencing (NGS) and further bioinformatic analysis.[3] In recent years, numerous variations have been developed, such as immunoprecipitation-coupled SELEX (IP-SELEX),[40] capillary electrophoresis-SELEX (CE-SELEX),[41] *in vivo*-SELEX,[42] and atomic force microscopy-SELEX (AFM-SELEX).[43] The various assays and methodologies for the selection of aptamers largely depends on the specific target of interest. As a result, each of these SELEX modes is tailored to fit the requirement of specific purpose for the individual target.

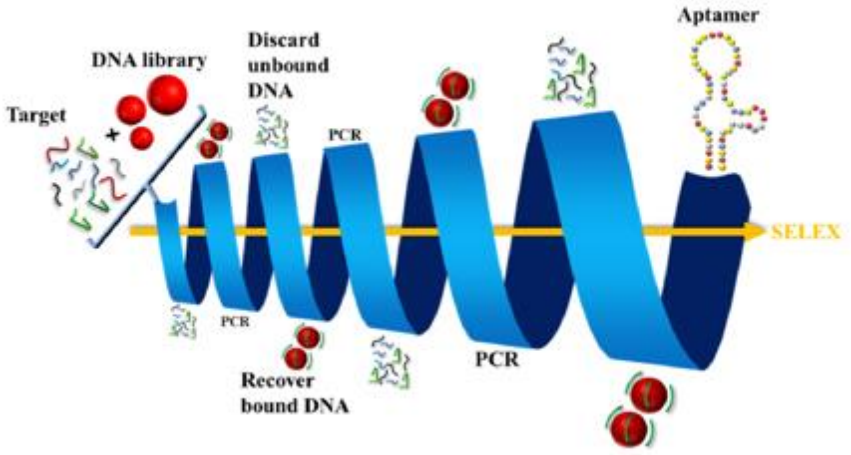

Figure 1.5 Schematics of SELEX workflow.[18]
An initial DNA library is incubated with the target of interest. The unbound sequences are washed and discarded. Bound sequences are recovered and amplified to become the library for subsequent rounds. After iterative rounds of SELEX, the pool is sequenced, and the most represented candidates are tested for their binding to the target.

To maximize the chance of successfully identifying aptamers of interest, the design of SELEX protocol requires careful considerations, including but not limited to the type and modification of initial libraries, design of negative and counter selection, the ramp of selection

pressure or stringency, accessibility to instruments, as well as cost optimization, efficiency, and time.[44]

An initial library with equal distribution motifs of all four nucleotides is critical in maximizing the sequence space to be explored. Aptamers are typically composed of a 20 - 60 nucleotides (nt) random region flanked by two 18 - 25 nt long fixed regions. While a shorter random region will maximize the coverage of the entire sequence space, a longer random region will provide more diverse possible 3D structures and folds.[45] For instance, a library with 40 nt of random sequence has 4^{40} (approximately 10^{24}) possible combinations. The fixed regions are designed for primer annealing and PCR amplification. In most cases, two fixed regions are complementary to one another so that a stem will form for the proper 3D folding of aptamers.

There are multiple ways to incubate the aptamer pool with targets. Targets could be immobilized on a surface, or without support if the targets are whole cells or implemented *in vivo*. Methodologies of incubation are critical since they are directly associated with methods to efficiently separate the bound from unbound sequences. While SELEX utilizing solid-phase support is mainly used to select for protein of interest, another SELEX protocol, cell-SELEX,[46] could be used to target whole cells. Several advantages have made cell-SELEX a promising strategy over recent years: Aptamers that target different types of cells or same type of cells at different stages can be differentiated via cell-SELEX, which can have great potential for developing cell-mediated therapies.[47] Moreover, cell-SELEX can also be tailored to select for proteins in their native states. The issue that aptamers selected from pure protein molecules may not be able to bind to the same proteins in their endogenous state is circumvented.

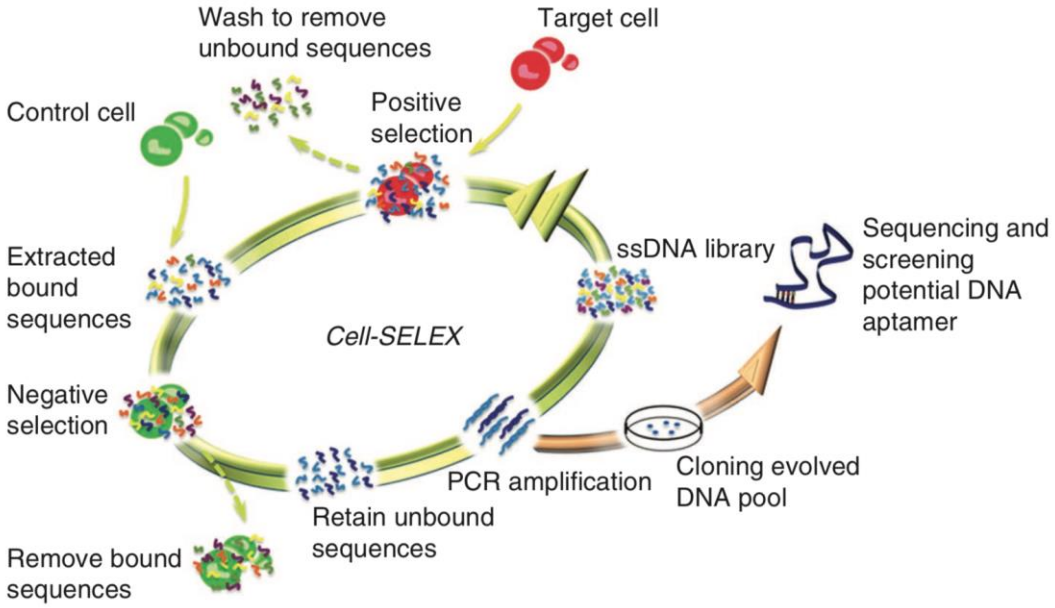

Figure 1.6 Schematics of cell-SELEX workflow.[46]

The initial ssDNA library goes through positive, competitive, and/or negative selection in one round to retain the sequences with specific recognition ability to target cells. The sequenced pools are cloned and and the positive clones are sequenced to identify individual aptamers.

The amplification step of the SELEX protocol is achieved via PCR-amplifying. The goal is to enrich for only the selected sequences with demonstrated strong binding to the target of interest for the next round, which usually involves two steps: analytical PCR, and preparative PCR.[46] Analytical PCR determines the optimal number of cycles by testing on a small sample of aptamer pool with incrementing cycle numbers. The majority of the aptamer pool will then be amplified during preparative PCR with the determined optimal number of cycles. The optimal number for PCR should yield the highest concentration of PCR product without introducing PCR by-product. It is a tradeoff between reducing the number to decrease the non-specific amplicons and maintaining enough product for the next round of SELEX.

The last step of SELEX protocol is the separation of single-stranded (ss) DNA from the double-stranded (ds) PCR amplified product, which is critical for a successful aptamer selection procedure. Several ssDNA separation methodologies including asymmetric PCR, magnetic

separation with streptavidin-coated beads, Lambda exonuclease digestion, and denaturing Urea-PAGE gel separation have been developed and broadly used by various groups.[48] Streptavidin-coated beads is by far the most widely used method due to its easy implementation and efficiency. A biotinylated primer is used so that one strand of the ds aptamer product is biotinylated during PCR. The aptamer product is then attached on the streptavidin beads, so that the non-biotinylated strand can be separated by alkaline denaturation.

1.2 APTAMER IN CANCER THERAPEUTICS

In view of their high binding affinities, specificities, and numerous advantages discussed above, aptamers have been applied in a variety of applications in the field of molecular biology, biotechnology, and biomedicine, environment monitoring, and even food science.[3,4] Especially in the field of cancer therapeutics, aptamers have great potential as agents for diagnostics, drug delivery, or even directly applied as treatments. For instance, aptamers have been developed for the detection of a number of cancer-related proteins, such as IGHM for Burkitt's lymphoma,[49] and STIP1 for ovarian cancer.[50] Aptamers have also been developed for recognizing whole cancer cells, including MCF-7, breast cancer cells[51] and CCRF-CEM, leukemia cells.[52] With an exponentially increasing number of related publications, the field of aptamer-mediated therapeutics embody a promising future for cancer diagnosis, prognosis, and treatments.

1.2.1 *Brain Tumor and Brain Metastases*

Primary brain cancer are abnormal growth of tissue that starts in the brain or the central nervous system (CNS). [53] Malignant brain tumors are one the most aggressive and intractable types of cancer. In population aged 0 - 14 years old, brain and other CNS tumors were the most common cancer site and most lethal of all solid tumors.[54] Children who survived brain tumor and entered

adulthood still often suffered from long-term consequences of exposing the developing brain to medical interventions.[55] Among all primary brain tumors, Glioblastoma (GBM) is the most common and aggressive type. Classified as grade IV gliomas, GBM is characterized with an extremely infiltrative growth and heterogeneous tumor microenvironment (TME).[56,57] Upon diagnosis, more than two-third of the adults survive less than 2 years and less than 6% pass 5-year survival.[54] Primarily diagnosed in the elderly population with a median age of 64.[54] The incident rate rises with increasing age, peaks at 75 to 84 years and drops after 85 years.[54] With a growing aging population, the number of cases is expected to significantly increase.

Brain metastases are cancerous tissues that originate from other parts of the body and later spread to the brain through bloodstream and lymphatic vessels.[53] Metastases most commonly arise from melanoma, breast, and lung cancers.[58] Approximately 10 - 35% of patients with primary tumors originate other than the brain later develop brain metastases.[59] This population accounts for 150,000 to 200,000 annual brain metastases cases. They are also becoming more common as rapidly developing treatments prolongs the survival time for cancer patients, allowing more time for cancer to spread.

The typical standard of care for brain tumors is maximal surgical resection with preservation of neurologic function, followed by adjuvant radiation therapy.[60] However, these treatments are minimally effective, especially in the case of aggressive malignancies like GBM. Moreover, for patients developing brain metastases, surgery is often not applicable as multiple lesions are present in the brain. As a result, these limited strategies are usually associated with high mortality rates and poor prognosis.[61] Improvements in patient survival are measured in weeks or months.[62] As cases of brain tumors and brain metastases continue to increase, there is an urgent need for novel therapies to effectively arrest the progression of tumorous cells in the brain.

1.2.2 *Blood-Brain Barrier: structure and solute transport*

A critical factor that lead to the minimally effective current treatments of brain cancers is the lack of accessibility of drugs to the brain via the intravenous route. The pathway is restricted by the blood-brain barrier (BBB), one of the most essential protection mechanism for the CNS.[63] It is a highly restrictive barrier which limits the movement of 98% of small molecules from entering the brain and disrupting homeostasis.[64] The BBB selectively allows individual molecules such as small lipid-soluble molecules to pass through the endothelial membrane while limiting the passage of pathogens or toxins.[63] However, it also becomes a major obstacle when diseases take place in the brain since it dramatically hinders the delivery of drugs and infiltration of some immune cells to the site. Therefore, an effective pathway across the BBB must be achieved for non-invasive brain cancer treatments.

The BBB consists of endothelial cells lining the brain vasculature along with astrocytes and pericytes (**Figure 1.7 B**).[65] Tightly connecting these endothelial cells are two main types of junctional proteins: tight junctions (TJ) and adherent junctions (AJ) (**Figure 1.7 C**).[66] These junctions significantly reduce the permeation of ions and other small hydrophilic solutes via the paracellular pathway, forming a physical barrier for transport to be tightly controlled via the transcellular pathway.[63] Both the highly polarized BBB endothelial cells and these junctional complexes significantly limit the free transportation of molecules into the brain.[65] Moreover, protein efflux transporters like P-glycoprotein (P-gp), and multidrug resistance protein-1 and 2 (MRP-1 and MRP-2), are highly expressed on the endothelial cells membranes, strictly preventing transport of molecules greater than 500 daltons.[67,68]

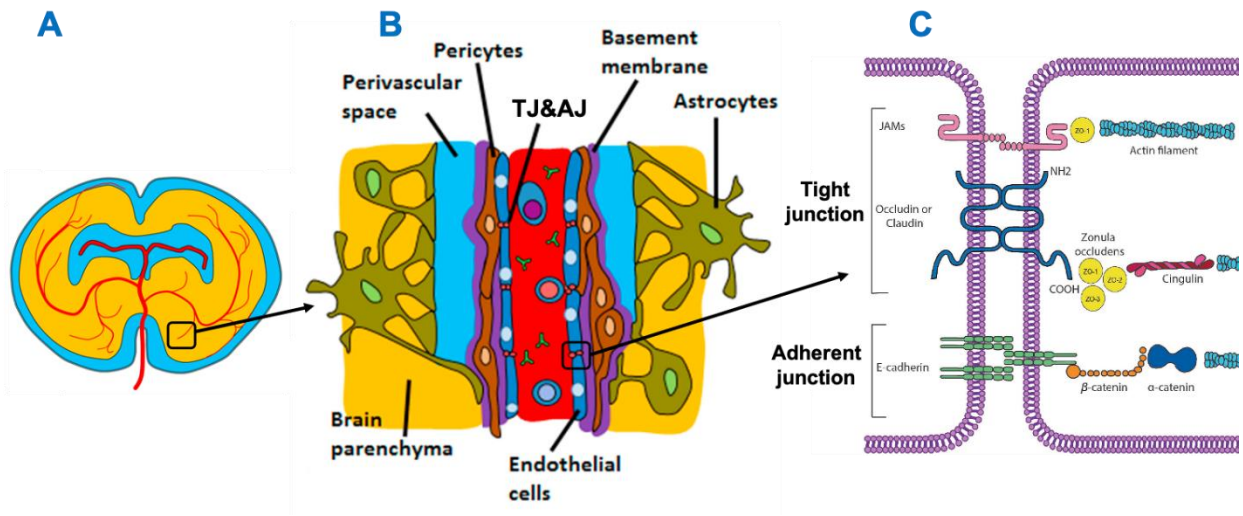

Figure 1.7 Structure and components of the blood-brain barrier.
A. Coronal view of the human brain.[69] B. Blood-brain barrier is formed by the small blood capillaries infiltrating into deep structure of the brain. The capillaries are lined with polarized endothelial cells connected with junctional complexes. On the abluminal side of the barrier these cells are lined by surrounding astrocytes and pericytes.[69] C. Components of junctional complexes.[70] Tight Junctions (TJ) are comprised of three integral transmembrane proteins, occludin, claudin and junctional adhesion molecules interconnected with accessory proteins. Adherent junctions (AJ) provide structural support for holding adjacent endothelial cells together.

BBB tightly controls the influx of vital molecules, and minerals essential for the maintenance of brain homeostasis while keeps out toxins to minimize neural cell death.[71] The mechanism of transportation is limited to transcellular transport including passive diffusion, carrier mediated transport (CMT), receptor mediated transcytosis (RMT), and adsorptive-mediated transcytosis (AMT), as well as paracellular transport, which only permits few water-soluble molecules (**Figure 1.8**).[69,72,73] The passive diffusion is driven by concentration gradients and only allows small hydrophobic molecules. CMT is the critical pathway for the passing of polar molecules such as glucose, amino acids, and nucleosides. Carriers on the apical surface recognizes their cargo, transport them into the endothelial cells by facilitative diffusion.[74] Proteins on the basal membrane then transport the cargo into the brain parenchyma.[74] The AMT provides a pathway for the uptake and transport of cationic molecules triggered by the electrostatic interactions between positively charged cationic molecules and negatively charged membrane surface domains.[75]

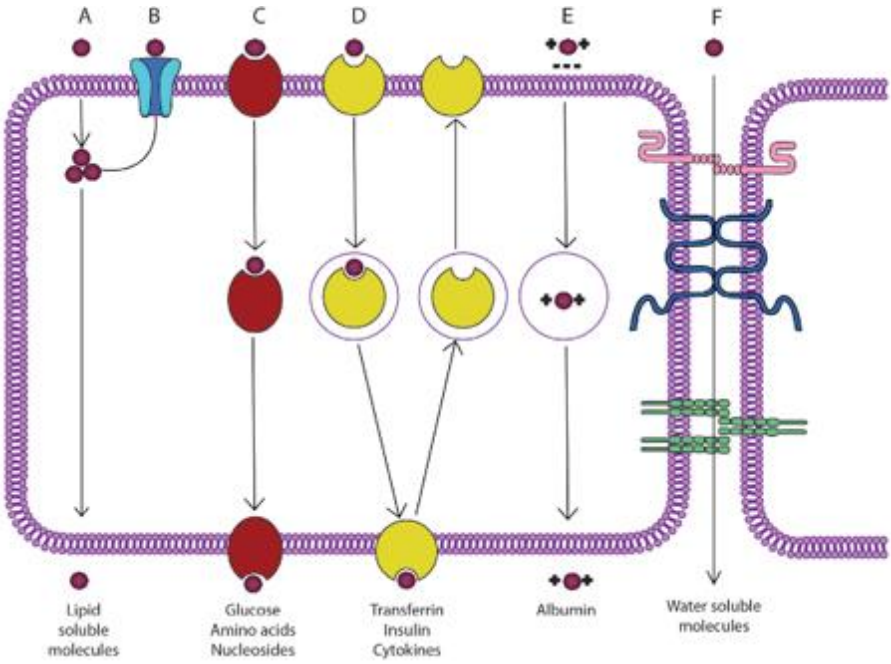

Figure 1.8 Transportation mechanisms across the BBB.[70]
Transcellular transport: A. Passive diffusion; B. ATP-binding cassette transporter efflux; C. Carrier mediated transport (CMT); D. Receptor mediated transcytosis (RMT); E. Adsorptive transcytosis; F. Paracellular transport.

RMT is the main pathway for the entry of large macromolecules. Compared to AMT, which is a non-specific pathway, the internalization of proteins via RMT is highly specific. This mechanism permits the transport of endogenous proteins up to 80 nm in diameter.[76] After the protein is bound to the receptor on the apical plasma membrane, the membrane invaginates the complex and forms an intracellular vesicle via endocytosis. Then, the vesicle is either recycled back to the apical plasma membrane or shuttled to the basolateral plasma membrane to release the cargo. Serum proteins that utilize RMT pathway includes transferrin (Tf), insulin, low-density lipoproteins receptor (LDLR), and low density lipoprotein receptor–related proteins 1 (LRP1) and 2 (LRP2).[77]

Utilizing RMT for drug transportation is a non-invasive strategy for drug delivery into the brain that offers significant advantages.[73,78] Compared to strategies that directly bypass or temporarily disrupt the BBB, utilizing endogenous pathways causes minimal to no disruption and

can target multiple cancer sites as well as the deeply infiltrated cancerous tissues. Moreover, compared to AMT-associated drug delivery, which relies on positively charging the cargos, RMT offers specific delivery with less off-target effects.[79]

1.2.3 *Transferrin and Transferrin Receptor*

Over the past 30 years, RMT has been of high interest for the delivery of different therapeutics including but not limited to antibodies, nanoparticles, and nucleic acids.[73,78] The most explored pathway for brain endothelial cells is the transport of iron delivery, which is achieved via the binding and trafficking of iron-loaded transferrin (Tf) and transferrin receptor (TfR, also known as CD71). Iron plays a critical role in maintaining the normal brain function, including mitochondrial energy generation, neurotransmission, oxygen transport, and cellular division.[80] It is an attractive route for drug delivery purposes and cancer therapeutics due to the elevated expression of TfR on brain endothelial cells and on cancer cell lines.[81]

The 76 kDa Tf molecule consists of a single polypeptide chain with two domains, C lobe (Tf-C) and N lobe (Tf-N) (**Figure 1.9**). Each domain has one iron-binding site, so each Tf can carry two iron atoms. Tf without iron bound is referred to as apo-Tf; Tf with one iron is referred as mono-ferric Tf; Tf with two iron molecules is referred to as di-ferric Tf, or holo-Tf.[82,83] At physiological pH of 7.4, the binding affinity of Tf to iron is extremely high that the binding is almost irreversible[84]. When the pH is lower than 6.5, the K_d significantly increases, leading to the release of iron.[85] Therefore, essentially all iron molecules stay bound to Tf in the plasma.[86] Since Tf is of high abundance, only about 30% of the Tf molecules are saturated with iron in the plasma.[86]

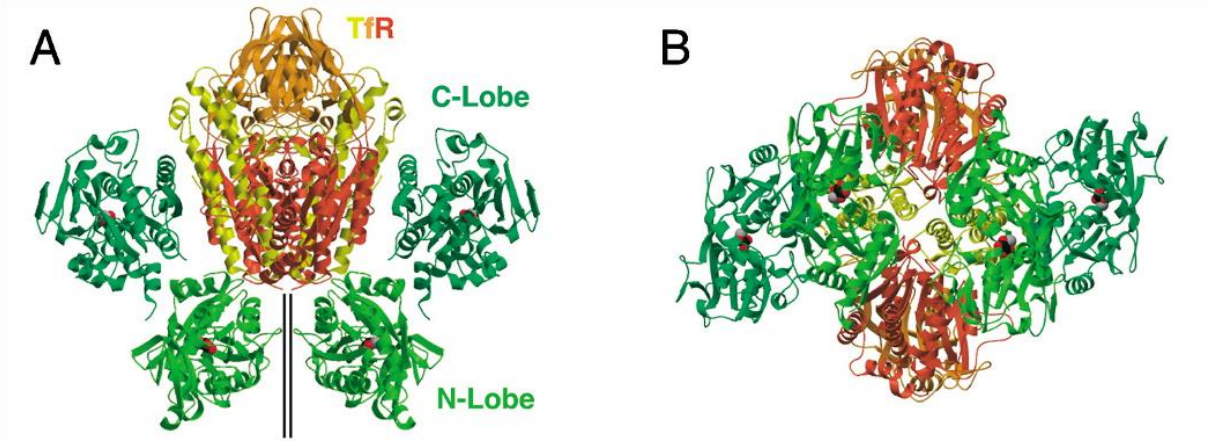

Figure 1.9 Structure of transferrin receptor/holo-transferrin complex.[87]
A. Face-on view B. bottom view of the atomic model of the TfR/holo-Tf complex. Holo-Tf is composed of two domains: C-lobe (dark green) and N-lobe (light green). Each TfR can bind to two holo-Tf molecules. Each holo-Tf can hold two iron molecules. TfR has three domains: a protease-like membrane domain (red), a helical domain (yellow), and an apical domain (orange).

There are two types of TfRs, TfR1 and TfR2. While TfR2 is mainly expressed in tissues in the liver and small intestines, TfR1 is generally found on the surface of most body cells,[83] and is one of the most widely explored protein target for targeted drug delivery to the brain. The 180 kDa TfR1 (short as TfR or CD71) is a transmembrane protein composed of two monomers joined together by two disulfide bonds. Each monomer has three domains: a protease-like membrane domain, a helical domain, and an apical domain (**Figure 1.9**).[87] The crystallized Tf-TfR complex shows that, while Tf-C interacts with the helical domain of TfR, Tf-N extends toward the membrane and inserts into the gap between large TfR ectodomains and the membrane surface.[87]

The exact mechanism of TfR-mediated iron delivery across the BBB is still under debate between two theories.[88] Both theories agree that iron-loaded holo-Tf binds to TfR and enters the endosome by clathrin-mediated endocytosis.[89] The first theory (**Figure 1.10 left**) suggests that, due to the lowering of pH, the affinity of iron atoms to Tf protein is reduced, leading to the release of iron atoms in the endosomes.[90] While the released iron (Fe^{3+}) is reduced to ferrous iron (Fe^{2+}) and transported to the cytoplasm by divalent metal transporter 1 (DMT1), the TfR/apo-Tf complex

either recycles back to the apical membrane or stores inside the endothelial cells.[91] The ferrous iron will either be stored inside the cells, or pumped into the brain parenchyma by the iron exporter, ferroportin.[92,93] Ferroxidases, such as hephaestin and ceruloplasmin reside at the membrane of endothelial cells, pericytes, and astrocytic end-feet will oxidize iron back to its ferric state.[92,93] Moreover, studies have also showed that the main fraction of iron transported to the brain is protein bound and sensitive to DMT1 inhibition.[94] Tf is locally produced in the CNS and in the brain capillary endothelial cells,[86,95] suggesting the possible release of protein-bound iron from the intracellular pool of Tf molecules in the brain endothelial cells. The second theory (**Figure 1.10 right**) suggests that iron atoms do not get released in the endosomes and that DMT1 is not involved in the process. Same to what is proposed in the first theory, holo-Tf binds to TfR and is internalized into endosomes. The endosomes then translocate to the abluminal membrane of the cells to deliver holo-Tf to the brain parenchyma.[96,97]

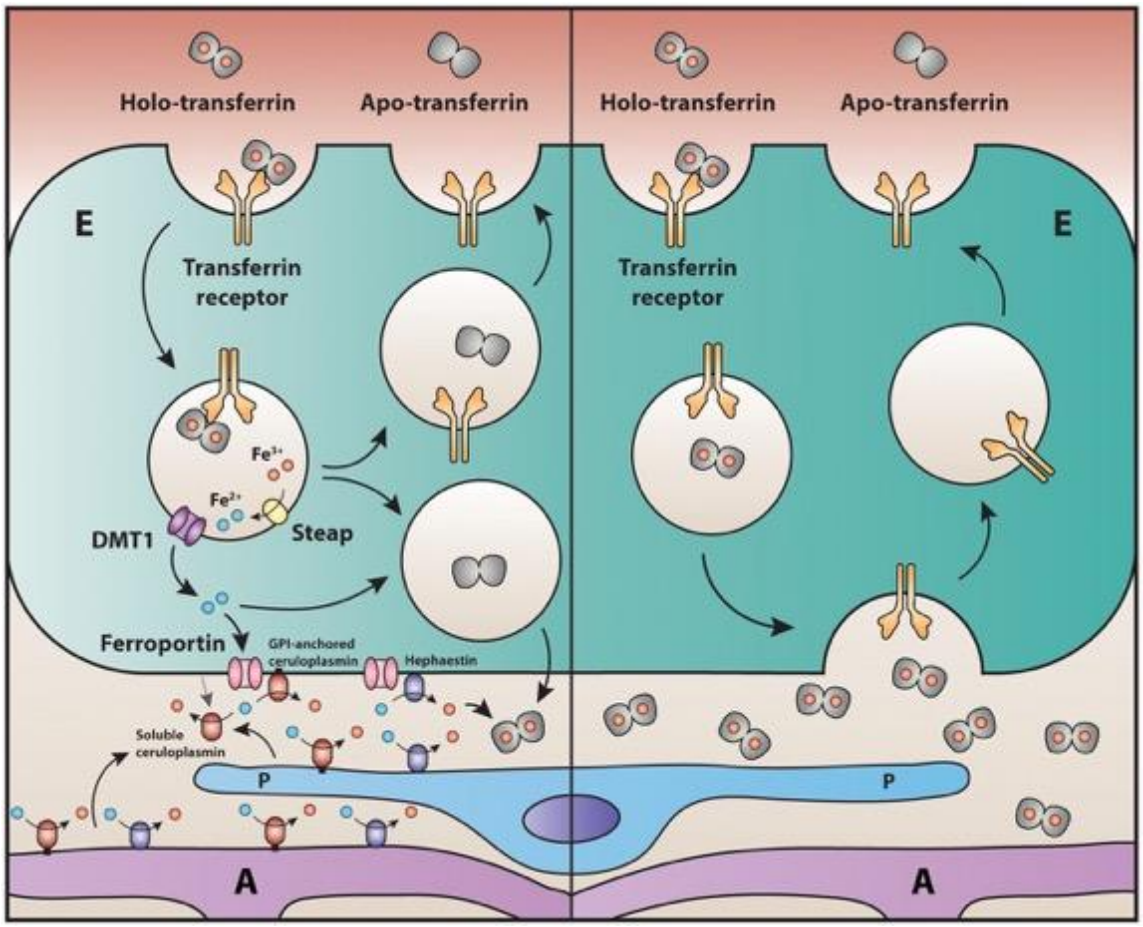

Figure 1.10 Two mechanisms proposed for iron delivery across the BBB.[98]
The first model (left) involves endocytosis of the TfR-Tf complex, dissociation of Tf protein due to pH reduction, and reduction of ferric iron to ferrous iron. The reduced iron will be transported out of the endosome membrane via DMT1 and pumped into the brain parenchyma by ferroportin. The second model (right) involves transcytosis of the TfR-Tf complex across the cell to deliver Tf protein to the brain parenchyma. E: brain capillary endothelial cells; P: pericytes; A: astrocytic end-feet.

1.3 Conclusions and Thesis Organization

Aptamers are single-stranded nucleic acid sequences capable of recognizing and binding to targets with high affinity and specificity. Considered as functional counterparts to antibodies, aptamers possess various advantages, such as small size, easy production and modification, and low immunogenicity. These advantages make them attractive for various applications ranging from therapy, drug delivery, diagnosis to biosensing. Aptamers are generated via SELEX. Extensive

work had been done to continue improving the *in vivo* stability of aptamers as well as the efficiency of SELEX methodologies.

Treatment of brain and CNS disorders remains the holy grail in the field of drug delivery due to the obstacle imposed by the BBB. Due to their elevated expression on brain endothelial cells and the potential for macromolecule delivery, the Tf/TfR receptor system have been the subject of intense investigation for several decades. The exact mechanism of the intracellular sorting of the TfR in brain endothelial cells is still under debate. A number of studies have demonstrated therapeutic outcomes in the brain in preclinical models using Tf/TfR-targeting molecules. However, the translational outcomes in clinical settings of these studies have been limited.

Here, we presented our expansive effort in developing aptamers for the treatment of brain diseases. We showed the process of adapting and integrating various strategies for the discovery of Tf protein via protein-SELEX (**Chapter 2**). We then demonstrated the characterization, cross-reactivity, and potential applications of a TfR (CD71) binding aptamer (**Chapter 3**).

Chapter 2. DEVELOPMENT OF TRANSFERRIN BINDING APTAMER

Abstract

Compared to the vast majority of studies that utilizing transferrin receptor (TfR, also known as CD71), fewer studies have investigated on the conjugates made of transferrin (Tf) for drug delivery to the brain, as high concentration of serum Tf in the circulation would compete for the TfR binding. We propose a novel construct that directly targets the endogenous Tf using aptamers. In particular, the goal of the project is to discover a high-affinity Tf-binding aptamer via SELEX. We present our expansive effort in the development and improvement of various SELEX strategies, including target-immobilization SELEX and a new protein/cell combinatorial SELEX. We also analyze the raw aptamer sequences from next-generation sequencing (NGS) and evaluate the partition efficiency of centrifugal separation. The total 17 rounds of SELEX reveal that implementation of negative selection, careful control of the stringency, and efficient partitioning of the pool are key aspects for a successful SELEX.

2.1 INTRODUCTION

Plenty of studies have been researched on targeting transferrin receptor (TfR, also known as CD71) for drug delivery in the past 30 years.[69,72,76,81,98] Attempts were also made to develop constructs designed with the receptor ligand, transferrin (Tf), as a targeting molecule. For instance, a diphtheria toxin conjugated Tf (Tf-CRM107) for the treatment of malignant gliomas had proceeded to phase III clinical trial, suggesting such administration routes to be highly promising.[99,100] However, fewer studies have investigated on the conjugates made of Tf for drug

delivery to the brain and cancer tissues. One potential factor is that large amounts of endogenous Tf in the circulation would compete off the exogenously introduced Tf for the TfR binding.[101]

To circumvent the issue of endogenous competition, instead of a protein-drug conjugate, we propose a novel design to directly target endogenous Tf for drug delivery to the brain. Such a construct must satisfy two considerations: First, the size of the cargo should be limited, as uptake of excessively large structures might distort the intracellular sorting mechanism of RMT.[97,102] Second, the binding of the cargo should not interfere with the normal binding of holo-Tf to TfR on the endothelial cells.

Compared to peptides and antibodies, aptamers are much smaller in size and easier to modify with drug conjugates. Their complex 3D structures also offer a variety of shape complementarity for specific targeting of the soluble protein. They are hence suitable for BBB delivery therapeutics via the iron-loading pathway. To this end, we hypothesize that a holo-Tf targeting aptamer will recognize and bind to holo-Tf protein with high specificity and affinity. The holo-Tf/aptamer complex will then bind to TfR on the apical plasma membrane of the brain endothelial cells, triggering endocytosis of the protein/aptamer construct for delivery into the brain parenchyma. The goal of this project is to develop aptamers that identify holo-Tf with high affinity and specificity via SELEX. Here, we present our expansive effort in the development and improvement of SELEX strategies, the analysis of NGS results, and the experience gained that enables future studies.

2.2 Material and Methods

2.2.1 *Materials and Reagents*

The unmodified anti-ssDNA library, ssDNA library, and PCR primers were purchased from Integrated DNA Technologies, Inc (IDT). 5-[(3-Indolyl)propionamide-N-allyl]-2'-deoxyuridine-

5’-Triphosphate was purchased from TriLink, 5-Indolyl-AA-dUTP, Tryptamino-dUTP analog. Unmodified nucleotides (dATP, dTCP, dCTP, dGTP) were purchased from QIAGEN. Thermococcus kodakaraensis (KOD) Hot Start DNA Polymerase (71086), KOD buffer, and the recombinant protein target holo (T0665) and apo (T1147) transferrin were purchased from Sigma-Aldrich. FITC transferrin polyclonal antibody (1:100, PA1-86736), Pierce™ high capacity Streptavidin agarose, Dynabeads® MyOne™ Streptavidin C1 magnetic beads, and Nunc Amino Immobilizer C8 strips were from Thermo Fisher. SpheroTM Streptavidin coated magnetic particles were from Spherotech.

Buffer Components. Surface Passivation (SP) buffer: 20 mM tris-HCl (pH 7.4), 140 mM NaCl, 5 mM KCl, 1 mM $MgCl_2$, and 1 mM $CaCl_2$ supplemented with 0.005% Tween 20. Stringent Wash (SW) buffer: 20 mM Tris-HCl (pH 7.4), 1 M NaCl, 5 mM KCl, 1 mM $MgCl_2$, 1 mM $CaCl_2$, 0.005% Tween 20. SB1T buffer: 40 mM HEPES, (pH 7.5), 125 mM NaCl, 5 mM KCl, 1 mM $MgCl_2$, 1 mM $CaCl_2$, 0.05% Tween 20. Washing buffer (WB): DPBS, 5.5mM $MgCl_2$, 4.5 mg/ml glucose. Binding buffer (BB): WB supplemented with competitors, including 0.1 mg/ml tRNA, different concentrations of BSA, and salmon sperm DNA.

2.2.2 *Target Immobilization SELEX*

A schematic of target immobilization SELEX procedure is shown in **Figure 2.2** and the conditions used in the individual rounds for the 1st attempt are summarized in **Supplemental Table 2.2**. The aptamer construct is consisted of a 40-nt-long random region (N40) flanked by two 20-nt-long fixed regions. Sequences of library and primers used are summarized in **Supplemental Table 2.1**.

Bulk Primer Extension for Round 1. The initial modified library with TrpdUTP was prepared by polymerase extension of a primer annealed to a biotinylated template, the anti-ssDNA library. 10 uM of library was added to primer extension reaction mix, which included 1uM

3’primer, 0.5 uM dATP, dCTP, dGTP and Trp-dUTP, 1X KOD DNA Polymerase Buffer, and 0.125 U/mL KOD DNA Polymerase.[21] The mixture was incubated at 68°C for 6-8 hours. The successful duplexes were then captured by incubation with Streptavidin Agarose resin for 30 min with rotation. The DNA pool was eluted by incubation with Sodium hydroxide (NaOH) for 5 min followed by neutralization with Hydrochloric Acid (HCl). The pool was buffer exchanged to SP buffer for further use.

Preparation of Target-Immobilization Plate. 100 nM of holo/apo-Tf recombinant protein was immobilized within wells of Nunc Amino Immobilizer C8 strips by incubating overnight at 4°C in 100 uL of 100 mM sodium phosphate (pH 7.5). Wells were washed 3 times with SP buffer and incubated with SP buffer for 1 hr under gentle agitation at room temperature (RT). Wells were washed again 3 times with SP buffer after incubation and stored at 4°C utill use.

Target Incubation with Aptamer Pool. 1 nmole of ssDNA pool in 100 ul of SP buffer was heated at 95°C for 5 min, then snap-cool on ice. The pool was then added to the functionalized, neutralized, and passivated well with protein, along with BSA and tRNA as competitors and incubated for a designated time period at RT under gentle agitation. After incubation, unbound and weakly bound aptamers were removed by 3 washes of SP buffer and 3 washes of SW buffer. The remaining members were eluted twice by incubation with 100 ul of 50 mM NaOH for 10 min at 70°C with agitation at 600 rpm, followed by neutralization with HCl. The solution was desalted using Amicon 10K centrifugal filters (Millipore).

Amplification of Selected Pool. The eluted ssDNA pool was amplified by PCR. The PCR settings were as follows: (i). 30s at 98°C. (ii). 10s at 98°C. (iii). 30s at 60°C. (iv). 30s at 72°C. (v). Repeat (ii) through (iv) for desired amount of cycles. (vi). Hold at 4°C.[46] Only the entire selected pool of the first round will be PCR amplified for 10 cycles. For the subsequent rounds, an analytical

PCR was performed to determine the optimal cycle that would yield a clear and bright electrophoresis band with no nonspecific amplicons. A preparative PCR was performed for amplifying the pool for the next round of selection.

Single-stranded DNA Isolation and Bulk Primer Extension. The separation of PCR product was achieved by separating biotinylated antisense ssDNA by alkaline denaturation and primer extension. The PCR product was incubated with Dynabeads® MyOne™ Streptavidin C1 beads at RT for 30 min with rotation. The non-biotinylated strands were then eluted by incubation with 20 mM NaOH at RT for 5 min followed by 3 washes with SB1T buffer. The beads with biotinylated antisense strands were resuspended in primer extension reaction mix and incubated at 68°C for 6-8 hours. Followed by 3 washes with SB1T buffer, the non-biotinylated strands with TrpdUTP were eluted with 20 mM NaOH for 1 min at 37°C with mixing followed by neutralization. The pool was buffer exchanged to SP buffer and quantified with Nanodrop (Thermo fisher) for the next round.

The same protocol was applied for the 2nd attempt of target immobilization SELEX (**Supplemental Table 2.3**) except for the following modifications: (1) Negative selection (1% BSA) was implemented at round 2 - 4; (2) During strand separation, the condition for elution of non-biotinylated strand switched from 20mM NaOH for 5 min to 200nM NaOH for 3 min; (3) Buffer exchange was implemented by NAP-5 DNA Purification Columns (GE HealthCare); (4) The concentration of reverse primer during primer extension was increased from 1uM to 10uM.

The same protocol was applied for the 3rd attempt of protein SELEX (**Supplemental Table 2.8**) except for the following modifications: (1) The entire SELEX proceeded with unmodified nucleotides. Regular dTTP, instead of TrpdUTP was used. (2) The primer sequences used for PCR amplification were FAM/FP/N40 and Biotin/RP/N40; (3) Streptavidin C1 beads and bulk primer extension with KOD polymerase were not implemented. FAM-labeled ssDNA were separated

from biotinylated antisense ssDNA by alkaline denaturation and affinity purification with Streptavidin Agarose Resin.[46]

2.2.3 *NGS Preparation and Analysis*

The starting library and ssDNA pools from SELEX round 1, 2 and 3 were PCR amplified with the barcoded primers listed in **Supplemental Table 2.4** for sequencing using the MiSeq Reagent Kit v2 (300 cycles) and MiSeq System (Illumina) according to the manufacturer's instructions. The variable regions of the sequencing results were processed from the raw data in two ways: (1) Trim to the variable region based on the specified length of the barcoded primers; (2) Trim to the variable region based on matching the sequences of the barcoded primers. Exported FASTA files were analyzed with FASTAptamer v1.0.3.[103] Specifically, FASTAptamer-Count was first used to determine rank and reads per million (RPM) for each sequence (**Supplemental Table 2.5**), whereafter FASTAptamer-Compare was used to conduct pairwise comparison of RPM for sequences between adjacent rounds and thus calculated fold enrichment (**Supplemental Table 2.6** & **Supplemental Table 2.7**).

2.2.4 *Combinatorial Protein/Cell SELEX*

Jurkat cell lines (ATCC) was cultured in RPMI 1640 medium (Gibco) with 10% heat-inactivated FBS (Life Tech and VWR). A schematic of the SELEX procedure is shown in **Figure 2.4** and the conditions used in the individual rounds are summarized in **Supplemental Table 2.9**. The ssDNA pool was heated at 95°C and snap-cooled on ice to allow proper folding. Negative selection was applied when the ssDNA aptamer pools were incubated with Trypsinized Jurkats or naive CD4 T cells for round 2 - 5 and round 6 - 7, respectively. The pool was then incubated with holo-Tf at molar ratio of 100:1 in BB at RT with rotation. The mixture was applied onto Amicon 100K

centrifugal filters and reconstituted in BB, followed by incubation with Jurkats at 4°C with rotation. After incubation, unbound and weakly bound sequences were removed by 3 washes of WB. PCR amplification and ssDNA isolation proceed as previously described.

2.2.5 *Round Binding*

Round binding studies were conducted with an Attune NxT (Invitrogen) flow cytometer. For target immobilization SELEX, Streptavidin-coated magnetic particles labeled with biotinylated target proteins were washed and incubated with folded FAM-labeled aptamer pool for 30 min at RT in SP buffer with 1%BSA at the indicated concentrations. Particles were washed twice in 500 µl of SP buffer with 1% BSA to remove excess unbound aptamer, and resuspended in 200 uL of SP buffer with 1% BSA before analysis via flow cytometry. For combinatorial protein/cell SELEX, folded FAM-labeled aptamer pool was incubated with target proteins before incubation with 2e6 Jurkats in BB at the indicated concentrations. Jurkats were washed twice in 200 µl of WB with 1% BSA to remove unbound aptamers, and resuspended in 200 µl of WB with 1% BSA before analysis via flow cytometry.

2.2.6 *Partitioning Efficacy*

An 80-nt-long FAM-labeled Jurkat binding aptamer (JBA) was used to predict the separation efficiency of the Amicon 100K centrifugal filters between protein-bound aptamers and the unbound. 400 ul of 500 nM FAM-JBA in BB was applied onto the column according to manufacturer's instruction (14,000 g, 10 min). The relative fluorescence units (RFU) values (Green) of the flow-through after each spin was measured using a fluorometer (Qubit) at fluorometer mode with excitation wavelength of 470 nm (Blue). The % flow through was calculated according to a standard curve matching serial dilutions of FAM-JBA to RFUs measured. The efficacy model was

constructed assuming that 30% of aptamers flows through after the first spin, 25% of remainder flows through in every next spin, and 10% stuck in the column.

2.3 Results and Discussion

2.3.1 *Target Immobilization SELEX*

To expand the chemical diversity of aptamers that bind to Tf protein, we functionalized natural nucleotides with protein-like properties by substituting dTTP with 5-tryptamino-dUTP (TrpdUTP) (**Figure 2.1A**) into the library during SELEX. TrpdUTP is a function analogous to Tryptophan (**Figure 2.1B**). This modification introduces hydrophobic surfaces on the aptamer and increases the chance of hydrophobic interactions with Tf, as hydrophobic interactions play critical roles in antibody-ligand bindings.[20] We incorporated a published SELEX protocol that selected for modified DNA aptamers from libraries incorporating dUTPs modified at the 5-position into our strategy (**Figure 2.2**).[21]

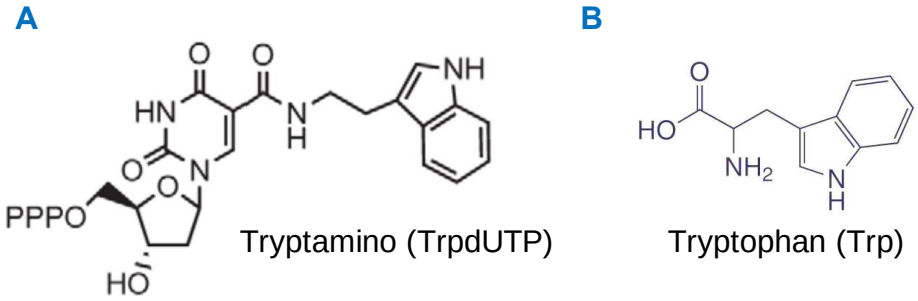

Figure 2.1 Chemical structures of Tryptamino and Tryptophan.[21]
A. Tryptamino (TrpdUTP) nucleotide; B. Tryptophan (Trp) amino acid.

The initial modified library with TrpdUTP was prepared by extension of primers annealed to a biotinylated anti-ssDNA library. The 40-nt-long random region contains 10^{14} to 10^{15} sequence variants. The target protein, holo-Tf was immobilized onto the immobilizer amino well plate followed by washes to neutralize and passivate the well. The aptamer pool was incubated in the

functionalized well, followed by wash of the unbound sequences and elution of the bound sequences with alkaline denaturation. The eluted sequences were amplified via PCR. An analytical PCR was performed to determine the optimal cycle that would yield a clear and bright electrophoresis band with no nonspecific amplicons. A preparative PCR was then performed to enrich for a sufficient amount for the next round of SELEX. The double-stranded (ds) PCR product was annealed to streptavidin-coated magnetic beads and non-biotinylated strands were eluted by alkaline denaturation. Single-stranded (ss) DNA strands with TrpdUTP for the next round were prepared by extension of primers annealed to biotinylated strands attached to the beads.

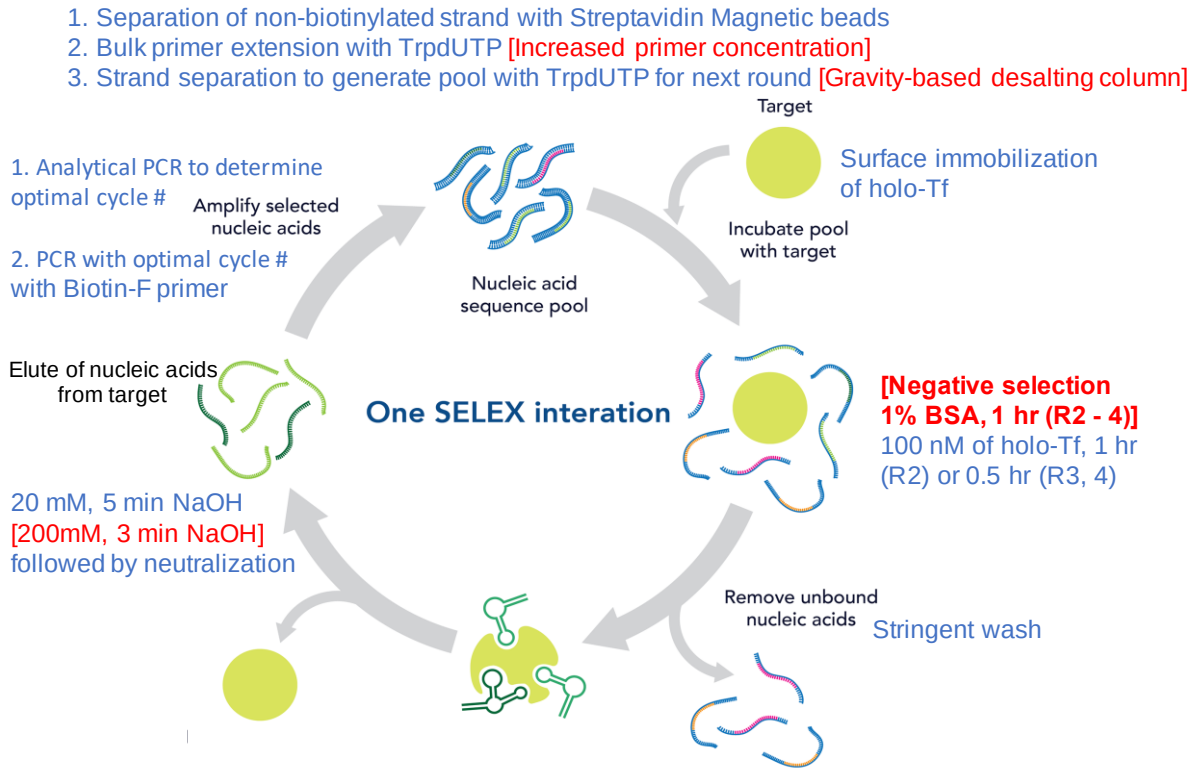

Figure 2.2 Workflow of target immobilization SELEX.
The DNA aptamer library underwent one round of positive selection against holo-Tf covalently immobilized onto a well, followed by three rounds of consecutive positive selection and negative selection against holo-Tf and 1% BSA, respectively, under increasingly stringent conditions. The differences between 1st and 2nd attempts are colored in red.

After an initial attempt rendered round 3 (R3) aptamer pool with no increased binding towards holo-Tf (**Supplemental Table 2.2**, **Supplemental Figure 2.7**), The following

modifications were applied in the second attempt restarting from R1 amplification pool: (1) A negative selection was implemented for subsequent rounds following R1. The pool was first incubated in well functionalized with 1% bovine serum albumin (BSA). The unbound pool was added to the holo-Tf functionalized well. The depletion of aptamers binding to undesired targets is critical for selecting for aptamers with high specificity. (2) During strand separation, the concentration and elution time of sodium hydroxide (NaOH) changed from 20 mM, 5 min to 200 mM, 3 min. A higher concentration of NaOH, when implemented within a shorter period, has been shown to successfully denature a higher percentage of dsDNA.[104] (3) Method for desalting in between rounds switched from DNA purification centrifugal filters to gravity-flow-based size exclusion columns. The latter has been utilized in a previously reported protocol with many demonstrated success.[46] (4) The concentration of reverse primer during primer extension was increased from 1 uM to 10 uM to ensure the maximal portion of the selected aptamer pool was preserved and carried onto the next round. Selection stringency in each of the four selection rounds was increased as summarized in **Supplemental Table 2.3**. An increased binding signal was detected from R3 aptamer pool on streptavidin magnetic particles coated with biotinylated holo-Tf protein (**Figure 2.3**). Selection was halted after four rounds due to the non-specific binding to control beads observed in round 4 (**Supplemental Figure 2.8**).

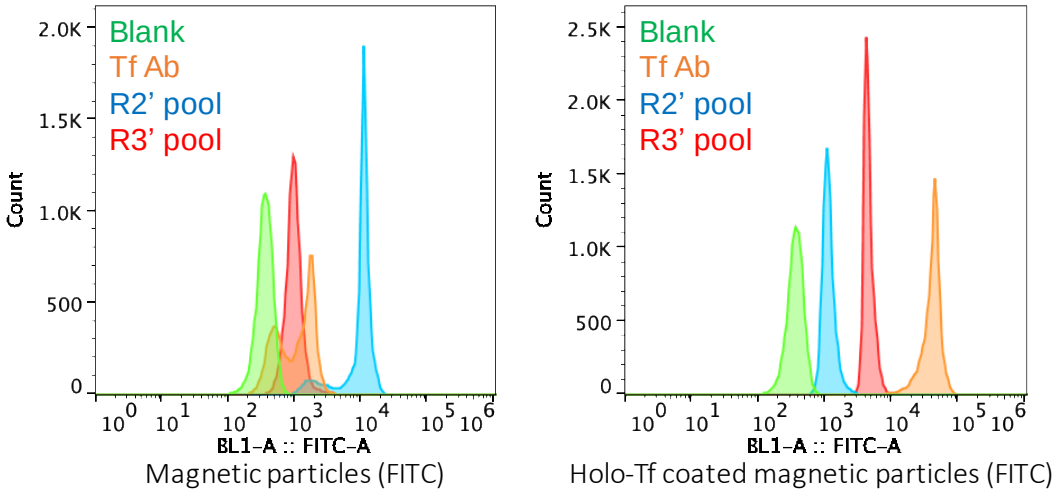

Figure 2.3 Binding of R3 aptamer pool from 2nd attempt of target immobilization SELEX. The flow cytometry histograms represent buffer-only blank (green), anti-transferrin antibody (orange), 200 nM nonspecific (NS) aptamer (blue), and 200 nM R3 aptamer pool (red) binding to a negative control, empty magnetic particles (left) and holo-Tf coated magnetic particles (right).

Aptamer pools from round 1, 2 and 3 were subjected to next-generation sequencing (NGS) using barcoded primers detailed in **Supplemental Table 2.4**. The raw sequenced data (100 bp) were processed by two methods for the identification of 40-nt-long random regions. One method is referred to as "hard-trimming"- trim to the variable region of aptamers based on the length of the flanking region. Since this method counts the number of nucleotides, this approach is left with random sequences all with lengths of 40 nt. Another method trims to the variable region based on matching the sequences of the flanking region. In this approach, the barcoded primer is aligned with each raw sequence, and the start of the random region is after the best alignment takes place. This method also renders the variable region, but allows any possible random region (from 1 to 99 nt) lengths to occur.

Theoretically, a successful NGS preparation and analysis would result in the same representation and distribution of processed sequences via two methods. However, by comparing processed results from both methods using FASTAptamer,[103] we noticed the most enriched

sequences processed via "hard-trimming" did not overlap with those processed via the second method (**Supplemental Table 2.6**, **Supplemental Table 2.7**). In other words, during NGS preparation and analysis, pieces of sequences without primer-recognized regions were mis-amplified and biased to become the most represented. The top three enriched sequences (**Supplemental Table 2.6**, **Supplemental Table 2.7 in red**) were fluorescein-labeled and subjected for binding studies with holo-Tf, apo-Tf, along with the R3 aptamer pool. The increased binding of the R3 pool was confirmed, yet no individual sequences showed binding to either holo-Tf or apo-Tf protein, which was consistent with the previous analysis (**Supplemental Figure 2.9**).

In an attempt to minimize PCR bias and non-specific amplicons introduced by primer extension, aptamer library without TrpdUTP was used to avoid the usage of KOD polymerase and to simplify the process in each round of SELEX. Moreover, SELEX for apo-Tf was implemented in parallel with the hope to distinguish the potential differences in selected aptamers. Selection stringency in each of the three selection rounds was increased as summarized in **Supplemental Table 2.8**. The SELEX was halted after three rounds due to the presence of non-specific bands shown on gel electrophoresis (**Supplemental Figure 2.11**).

The inconsistency between NGS analyses via two methods, as well as the non-specific amplicons in the later attempt, can be best explained by the generation of PCR by-products. PCR bias also exists towards shorter sequences or sequences that adapt better to the polymerases applied in the certain context. A major source of by-product is primer-primer hybridization, which leads to shorter ds PCR products.[105] Single-stranded sequences can also bind to complementary bases in the random region serving as a primer, which is then extended by the polymerase, yielding longer ds DNA products.[105] Due to the difference in properties such as GC content, secondary structures, and melting temperature, sequence adaption to DNA polymerase,

primers, and other PCR conditions, PCR amplification of a complex aptamer pool can be difficult.[106] Other non-specific amplification products resulting from the second round (barcoded-tagged) amplification, such as daisy chaining, or off-target amplification of contaminating template are also possible. Results from FASTAptamer analysis reveals that the total sequences of R3 shrunk by more than 50% compared to R2 (**Supplemental Table 2.5**). The sudden size decrease in library sequences from R2 to R3 supports the theory that PCR bias took place between rounds of amplification. The SELEX sequences could very likely fall into selecting sequences to fit best not to the target of interest but the PCR system.[107]

In the last attempt of SELEX starting from a library without TrpdUTP modification, natural nucleotides might not offer the chemical diversity and structural complexity required to construct aptamers that bind to holo-Tf with high affinity and specificity. Compared to the CDR loops on the variable domain of the antibodies, which hydrophobic interactions act as the main driving force for antibody-ligand binding,[20] the chemical interactions offered by natural nucleotides are limited to polar interactions such as van der Waals, hydrogen bonding, and electrostatic interactions. The SELEX was limited because there was a lack of successful candidates. When the sequences for amplification were scarce, the cycle number had to be high (**Supplemental Figure 2.11**), making the process prone to PCR defects. To some extent, the optimal cycle number of PCR indicates the stringency of the SELEX. The more cycles needed to yield a clear and bright electrophoresis band, the more stringent the SELEX strategy is. Since the amount of PCR products required for individual rounds of SELEX is fixed, a stringent SELEX might be the other reason for an unsuccessful attempt.

Other potential causes come from the solid phase immobilization methodology. During incubation, some sequences from the pool might inevitably bind to the surface of the wells

despite stringent passivation and neutralization, rendering non-specific sequences eluted from the well. Moreover, due to the chemical bonds required to immobilize protein on the surface, the protein might show a different shape and structure than from its native state. The selected aptamer might show binding profiles different from that of the immobilized protein.[108]

2.3.2 *Combinatorial Protein/Cell SELEX*

SELEX that involves the target immobilization process bears two limitations: First, non-specific binding of the aptamers to the immobilized surfaces is inevitable; Second, the selected aptamer might fail to bind its target in the native state, as the immobilized target could demonstrate a structure very different from that *in vivo*.[108] To circumvent the possible non-specific interactions that come with solid-phase immobilization SELEX, we developed a less stringent combinatorial protein/cell SELEX (**Figure 2.4**) that utilizes the endogenous Tf/TfR pathway incorporated in the strategy. The goal of the combinatorial protein/cell SELEX was to select for aptamer candidates that bind to holo-Tf in its native state without interfering with the endogenous Tf-TfR binding events.

The aptamer pool was first incubated with target protein, holo-Tf, in solution to allow a higher chance of binding to occur in its native state without chemical interactions due to the solid surface. The aptamer/Tf complex was separated from unbound aptamers via size cutoff columns before incubation at 4°C with Jurkats, an immortalized human T lymphocyte cell line that expresses a high level of TfR on the surface. After incubation, Jurkat cells were washed to remove any unbound aptamers. Bound sequences were eluted by heating the cell/protein/aptamer complex at 95 °C. The elevated temperature denatured proteins on the surface and disrupted secondary structures of aptamers, causing aptamer to release from the holo-Tf on the cell surfaces.[46] The eluted aptamer pool was then amplified by PCR. Sequences were separated from the biotinylated

antisense ssDNA by alkaline denaturation and affinity purification with streptavidin-coated Agarose beads.

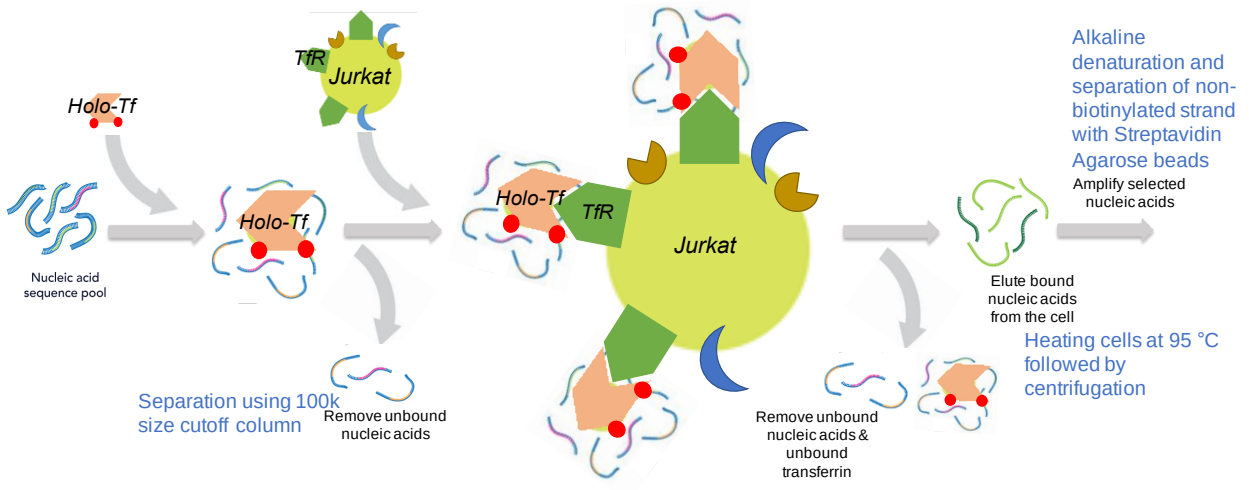

Figure 2.4 Workflow of the combinatorial protein/cell SELEX.
The DNA aptamer library was first incubated with holo-Tf in solution. Unbound sequences were removed and the holo-Tf/aptamer complex was incubated with Jurkats with elevated TfR expressed on the surface. Unbound complexes were removed by washing with WB. Bound sequences were eluted from the cells and PCR amplified for the next round.

In round 2 - 5, negative selection was performed by incubation of aptamer/holo-Tf complex with Trypsinized Jurkats (**Figure 2.5**). Trypsin is a serine protease that cleaves selective peptide bonds.[109] The loss binding of an aptamer that targets TfR has been observed on Jurkats pre-treated with Trypsin, suggesting loss of surface receptors on Trypsinized Jurkats. Since all healthy living cells express a certain level of TfR, negative selection for round 6 and 7 was performed on naïve CD4+ T cells. Selection stringency in each round was summarized in **Supplemental Table 2.9**. Selection was paused at R5 after a binding study performed on R5 aptamer pool showed no binding to holo-Tf (**Supplemental Figure 2.10**).

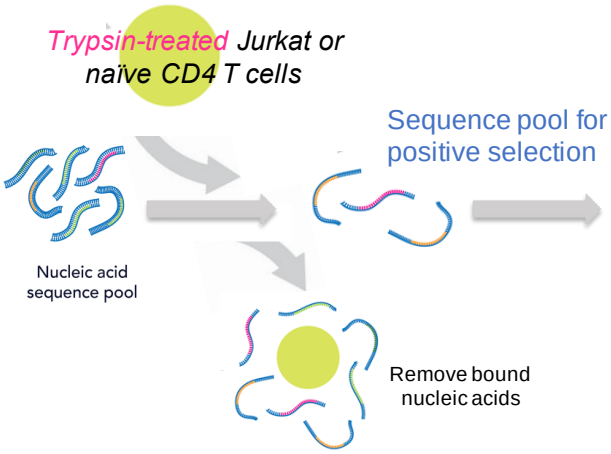

Figure 2.5 Negative selection of the combinatorial protein/cell SELEX.
The DNA aptamer library first underwent negative selection on Trypsin-treated Jurkats or naïve CD4+ T cells. Bound sequences were removed, and the unbound pool was ready for positive selection.

A retrospective study on column separation efficiency revealed that the inefficient separation between bound and unbound aptamers might be the reason that the round pool had not shown binding towards holo-Tf. Approximately 40-50% of ssDNA in the entire population were eluted after testing on the 100K size cut off column according to manufacturer's instructions (14,000 g, 10 min) (**Supplemental Figure 2.12**). While the molecular weight of the aptamer/protein complex is approx. 104k, the MW of unbound aptamer is approx. 26k. The difference was too small for the best performance of any size cutoff separation columns. Partitioning of bound sequences from the unbound sequences is critical in a successful SELEX, as SELEX relies on the evolution of the bound sequences along the process. Without efficient separation methods, a proportion of the aptamer pool when incubated with Jurkats, are not holo-Tf-bound.

We hypothesized that a proportion of aptamers have obtained binding affinity for holo-Tf by R5. However, the proportion was too small and not represented enough in the population for the entire aptamer pool to show binding. To this end, we proposed modifications of SELEX strategy to circumvent column separation as well as to maximize the chance of binding events to occur

between aptamers and holo-Tf. Excess amount of holo-Tf was pre-incubated with Jurkats to saturate the TfR on the cell surfaces. After negative selection on naïve CD4+ T cells, the aptamer pool was then incubated with holo-Tf-saturated Jurkats at 4°C in solution. The aptamer/Jurkats complex were then incubated in the media at 37°C for 30 min before Trypsinizing off surface TfR proteins. The purpose was to select for aptamers that were internalized into the cells. Selection was halted at R7 after a binding study performed on R7 aptamer pool showed no binding to holo-Tf (**Figure 2.6**).

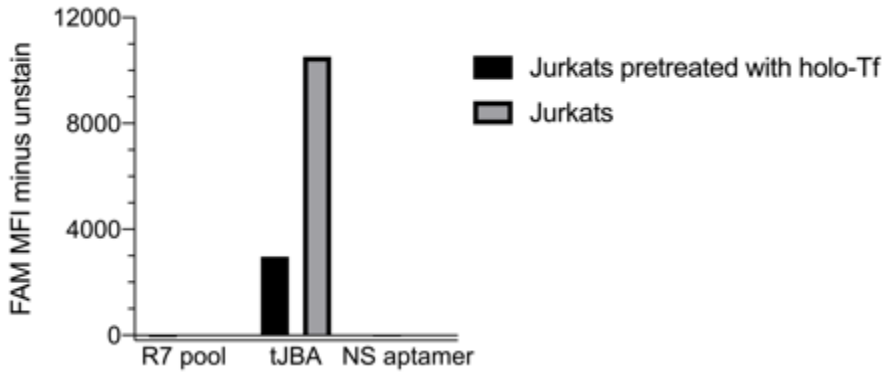

Figure 2.6 Binding of R7 aptamer pools from the combinatorial protein/cell SELEX. The bar represents the FAM median fluorescence intensity (MFI) of the R7 aptamer pool, a Jurkat binding aptamer, and a non-specific aptamer on Jurkats pre-incubated with excess (40 uM) of holo-Tf recombinant protein, or Jurkats.

Insufficient partitioning between the aptamer/protein complexes and unbound aptamers is the major cause to render aptamer pools with no binding affinity. Without efficient separation methods, unbound aptamers will accumulate via PCR after each round and gradually evolve to become the majority of the aptamer population. Furthermore, unmodified aptamers present limited stability at physiological temperature, as shown in previous studies.[10] Aptamers are prone to be non-specifically internalized by the cells at an elevated temperature.

2.4 CONCLUSIONS

Here, we demonstrated our expansive effort in developing SELEX variations and discovering Tf targeting aptamers. We presented a total of 17 rounds of SELEX with 3 attempts in target immobilization SELEX and 2 attempts in developing a novel combinatorial protein/cell combined SELEX. The most critical takeaways from this valuable learning experience are: (1) Implementation of negative selection is essential for the generation of a high specificity aptamer pool; (2) Stringency of SELEX design should be carefully controlled to minimize the chance for PCR by-product to present; (3) Efficient partitioning between bound and unbound sequences directly determines the success and efficiency of a SELEX.

2.5 SUPPLEMENTAL INFORMATION

Supplemental Table 2.1 Sequences of PCR Primers used for target immobilization SELEX and the combinatorial protein/cell SELEX.
Biotin/FP/N40 and FAM/RP/N40 were used for target immobilization SELEX. FAM/FP/N40 and Biotin/RP/N40 were used for combinatorial protein/cell SELEX. Text within slashes "/" represent IDT modification codes.

Name	Sequence
N40 library	5'- /52-Bio/TCG CTC TTT CCG CTT CTT CGC GG N40 CCG CGT AAG TCC GTG TGT GCG AA -3'
Biotin/FP/N40	5'- /5Biosg/TCG CTC TTT CCG CTT CTT CG -3'
FAM/RP/N40	5'- /56-FAM/TTC GCA CAC ACG GAC TTA CG -3'
FAM/FP/N40	5'- /56-FAM/TCG CTC TTT CCG CTT CTT CG -3'
Biotin/RP/N40	5'- /5Biosg/TTC GCA CAC ACG GAC TTA CG -3'

Supplemental Table 2.2 Experimental conditions in the 1st attempt of target immobilization SELEX.

SELEX round	Aptamer pool (μM)	Target protein: holo-Tf (μM)	Time (hr)	Negative selection	Competitor
1	14	0.1	1	None	None
2	0.5	0.1	1	None	0.1 mg/ml tRNA, 0.1% BSA
3	0.5	0.1	0.5	None	0.1 mg/ml tRNA, 1% BSA

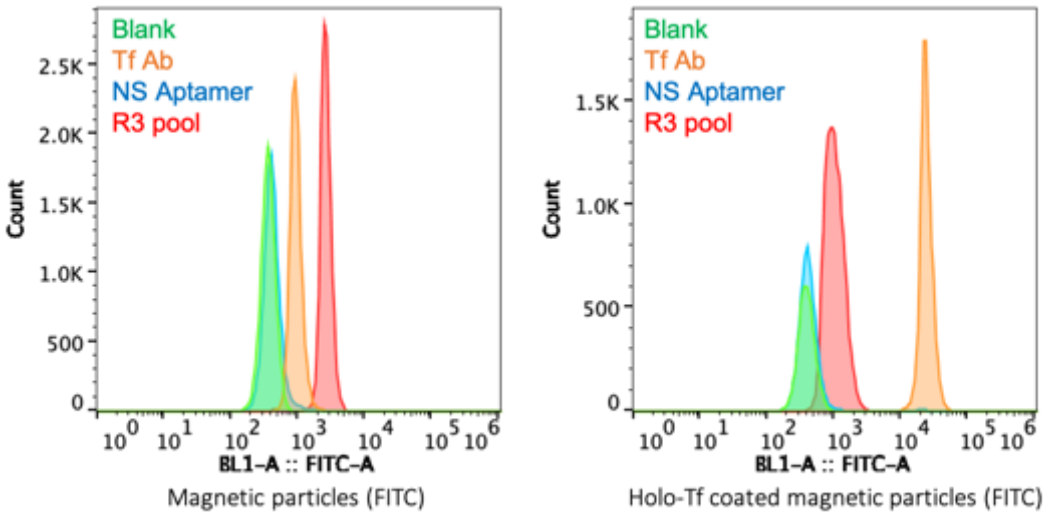

Supplemental Figure 2.7 Binding of R3 aptamer pool from 1st attempt of target immobilization SELEX.
The flow cytometry histograms represent buffer-only blank (green), anti-transferrin antibody (orange), 150 nM nonspecific (NS) aptamer (blue), and 150 nM R3 aptamer pool (red) binding to a negative control, empty magnetic particles (left) and holo-Tf coated magnetic particles (right).

Supplemental Table 2.3 Experimental conditions in the 2nd attempt of target immobilization SELEX.

SELEX round	Aptamer pool (µM)	Target protein: holo-Tf (µM)	Time (hr)	Negative selection	Competitor
1	14	0.1	1	None	None
2	0.5	0.1	1	None	0.1 mg/ml tRNA, 0.1% BSA
3	0.5	0.1	0.5	1% BSA, 1 hr	0.1 mg/ml tRNA, 1% BSA
4	0.25	0.1	0.5	1% BSA, 1 hr	0.1 mg/ml tRNA, 1% BSA

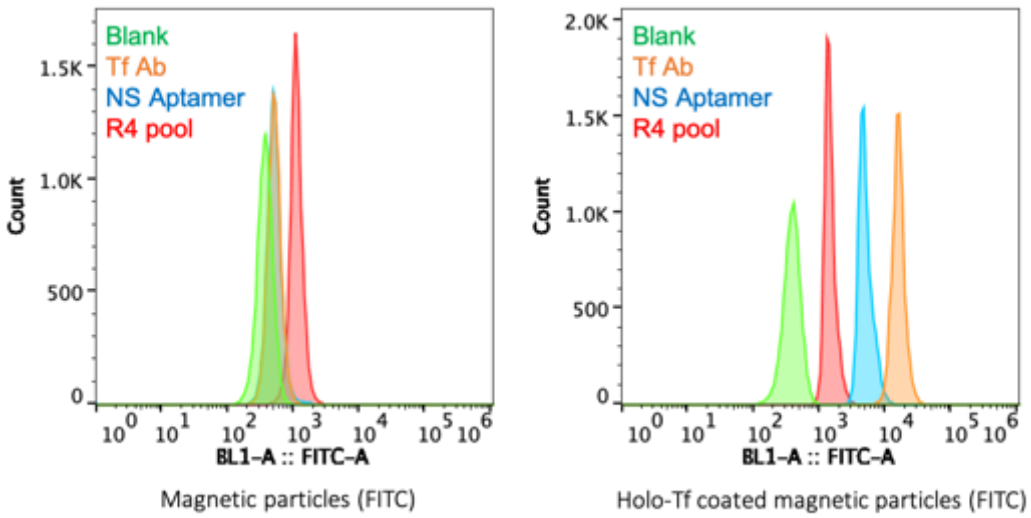

Supplemental Figure 2.8 Binding of R4 aptamer pool from 2nd attempt of target immobilization SELEX.
The flow cytometry histograms represent buffer-only blank (green), anti-transferrin antibody (orange), 150 nM nonspecific (NS) aptamer (blue), and 150 nM R4 aptamer pool (red) binding to a negative control, empty magnetic particles (left) and holo-Tf coated magnetic particles (right).

Supplemental Table 2.4 Primers used for next generation sequencing (NGS) of naïve library (NL) and 2nd attempt of target immobilization SELEX rounds 1-3.

Primer name	SELEX round	Sequence	Barcode (in red)
Aptamer_F_v2	NL, 1-3	AATGATACGGCGACCACCGAG ATCTACACACAGACCGTCGTC GCTCTTTCCGCTTCTTCG	
Aptamer_R_30v2	NL	CAAGCAGAAGACGGCATACGA GATtggtcagccaCGAGGAGATACC TTCGCACACACGGACTTACG	TGGCTGACCA
Aptamer_R_31v2	1	CAAGCAGAAGACGGCATACGA GATactatgcaatCGAGGAGATACC TTCGCACACACGGACTTACG	ATTGCATAGT
Aptamer_R_32v2	2	CAAGCAGAAGACGGCATACGA GATcgacgcgactCGAGGAGATAC CTTCGCACACACGGACTTACG	AGTCGCGTCG
Aptamer_R_33v2	3	CAAGCAGAAGACGGCATACGA GATgatacggaacCGAGGAGATAC CTTCGCACACACGGACTTACG	GTTCCGTATC

Supplemental Table 2.5 Number of total sequences and unique sequences counted from two NGS analysis methods.

	Trim to the variable region based on length of sequences		Trim to the variable region based on matching sequences	
SELEX round	**Total**	**Unique**	**Total**	**Unique**
NL	323543	314359	323528	317015
1	514948	497492	514919	501930
2	243943	50350	243920	63814
3	98630	39891	98602	48280

Supplemental Table 2.6 Top 10 R3 aptamer sequences of target immobilization SELEX ranked by reads per million (RPM) analyzed via "hard-trimming".
Fold enrichment is calculated by dividing RPM of the sequence from a round by the value of the former round. Sequences in red were ordered for the binding study

			Fold Enrichment		
R3 Rank	**% Representation**	**Sequence**	**R2/R1**	**R3/R2**	**R3/R1**
1	5.17%	TAGACGAAAAACATTGTTTTCC TGGAAGGCCCAGAATCTG	20.58	3.23	66.55
2	3.65%	TTACTAGATGCAACCCGACTAC TAACGTCGTAAGAGAGCC	29.58	6.36	188.14
3	3.45%	GGTCTAACTTTACCGCTACTAA ATGCCGCGGATTGGTTTC	3.43	3.23	11.09
4	3.35%	TCAAGGACTGTGTGACTATTGA CGTCCTTCCCCGTACGCC	7.18	4.8	34.46
5	3.35%	AATACGTGGCCTTATGGTTACA GTATGCCCATCGCAGTTC	2.49	6.28	15.66
6	3.24%	GATCGGTCTCGGCATTCCTGCT GAACCGCTCTTCCGATCT	5.43	4.4	23.87
7	2.84%	TCCAGCCACTTAAGTGAGGTGA TTTATGTTTGGTGCTATT	31.7	4.62	146.34
8	2.84%	GCAAGCACATCACCTTGAATGC CACCGGAGGCGGCTTTTT	2.74	5.33	14.62
9	2.74%	CCGTCAAGGACTGTGTGACTAT TGACGTCCTTCCCCGTAC	3.52	2.67	9.4
10	2.74%	GGCCTTATGGTTACAGTATGCC CATCGCAGTTCGCTACAC	7.04	3.34	23.5

Supplemental Table 2.7 Top 10 R3 aptamer sequences of target immobilization SELEX ranked by reads per million (RPM) analyzed via trimming to the variable region based on matching the sequences of the flanking region.
Untrimmed sequences (100 nt long) are deleted from the ranking. Sequence in red was ordered for the binding study.

			Fold Enrichment		
R3 Rank	**% Representation**	**Sequence**	**R2/R1**	**R3/R2**	**R3/R1**
3	2.64%	TGTGGTGCCTGGATACGGT	N/A	N/A	N/A
1269	0.91%	AAATGTGCCCTGTGGGCTTGGA ATGCCGGAGGAAGAAGAC	N/A	N/A	N/A
6010	0.41%	AAAAAATAGGCCGCGCCGAAA AAAATGGGACACGATAGTC	N/A	N/A	N/A
6010	0.41%	GAAACTAAACCGTACGCGAAA AAGCTCTTTGAAACAAACT	N/A	N/A	N/A
6010	0.41%	CCCCCACTAACTCGAGCGGTTA GAAGAGGGATCCATATGG	N/A	N/A	N/A
7426	0.30%	AAGGAAGAAGGACGATATCAG ATGAATCATATTGGAGGAAG	N/A	N/A	N/A
7426	0.30%	TGTAATAACTACGTAACAATAG AGAGTCCCAAGTCAGAAAG	N/A	N/A	N/A
7426	0.30%	TAACATCCGAGGCTATGAAAAG CGATTAGAAGAAAAGAGAC	N/A	N/A	N/A
7426	0.30%	GGTCTGCTCGTGCTCGATATTC TCAATGGGTGGAGTAATC	N/A	N/A	N/A
7426	0.30%	TATAAAAGACAGAGTGGGGCT AGAGGACACAGTGACCCAG	N/A	N/A	N/A

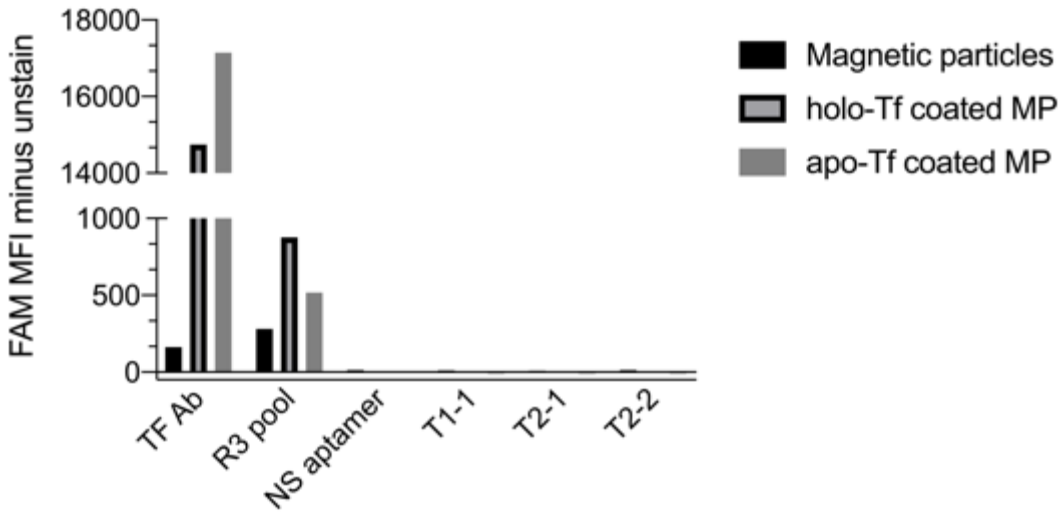

Supplemental Figure 2.9 Binding of top 3 enriched sequences from R3 of 2nd attempt of target immobilization SELEX.
The bar represents the FAM MFI of an anti-Tf Ab, R3 aptamer pool, non-specific aptamer, and 100 nM of the three aptamers termed T1-1, T2-1, and T2-2 on empty magnetic particles, holo-Tf coated magnetic particles, and apo-Tf coated magnetic particles.

Supplemental Table 2.8 Experimental conditions in the 3rd attempt of target immobilization SELEX.

SELEX round	Aptamer pool (μM)	Target protein: holo-Tf (μM)	Target protein: ap-Tf (μM)	Time (hr)	Negative selection	Competitor
1	14	0.1	0.1	1	None	None
2	0.5	0.1	0.1	1	0.1% BSA, 1 hr	0.1 mg/ml tRNA, 0.1% BSA
3	0.5	0.1	0.1	0.5	0.5% BSA, 1 hr	0.1 mg/ml tRNA, 1% BSA

Supplemental Table 2.9 Experimental conditions in combinatorial protein/cell SELEX.

R	Aptamer pool (μM)	Target protein: holo-Tf (nM)	Time (hr)	Separation w/ column (# of spin)	Cell	Negative selection	Competitor
1	14	140	1	2	10e6 Jurkats	None	0.1 mg/ml tRNA, 0.1% BSA
2	0.19	200	0.5	None	5e6 Jurkats	20e6 Trypsinized Jurkats	0.1 mg/ml tRNA, 0.1% BSA
3	0.3	3	0.5	None	5e6 Jurkats	20e6 Trypsinized Jurkats	0.1 mg/ml tRNA, 0.5% BSA
4	0.5	5	0.5	9	4e6 Jurkats	20e6 Trypsinized Jurkats	0.1 mg/ml tRNA, 0.5% BSA
5	0.25	2.5	0.5	9	2e6 Jurkats	20e6 Trypsinized Jurkats	0.1 mg/ml tRNA, 1% BSA, 0.1 mg/ml salmon sperm DNA
6	0.25	Excess on Jurkats	0.25	N/A	2e6 Jurkats	20e6 naïve CD4 T cells	0.1 mg/ml tRNA, 1% BSA, 0.1 mg/ml salmon sperm DNA
7	0.25	Excess on Jurkats	0.25	N/A	2e6 Jurkats	20e6 naïve CD4 T cells	0.1 mg/ml tRNA, 1% BSA, 0.1 mg/ml salmon sperm DNA

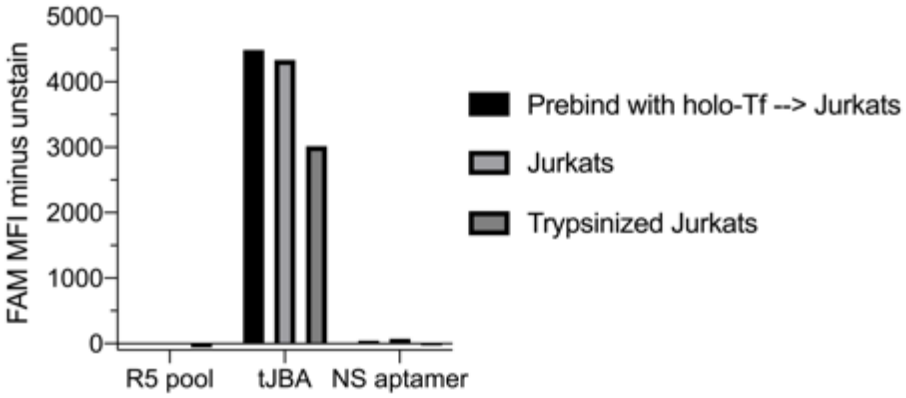

Supplemental Figure 2.10 Binding of aptamer pools from R5 of the combinatorial protein/cell SELEX.

The bar represents the FAM median fluorescence intensity (MFI) of the R5 aptamer pool, a Jurkat binding aptamer, and a non-specific aptamer on Jurkats or Trypsin-treated Jurkats. Aptamers were either pre-incubated with holo-Tf before incubation with Jurkats or directly incubated with Jurkats.

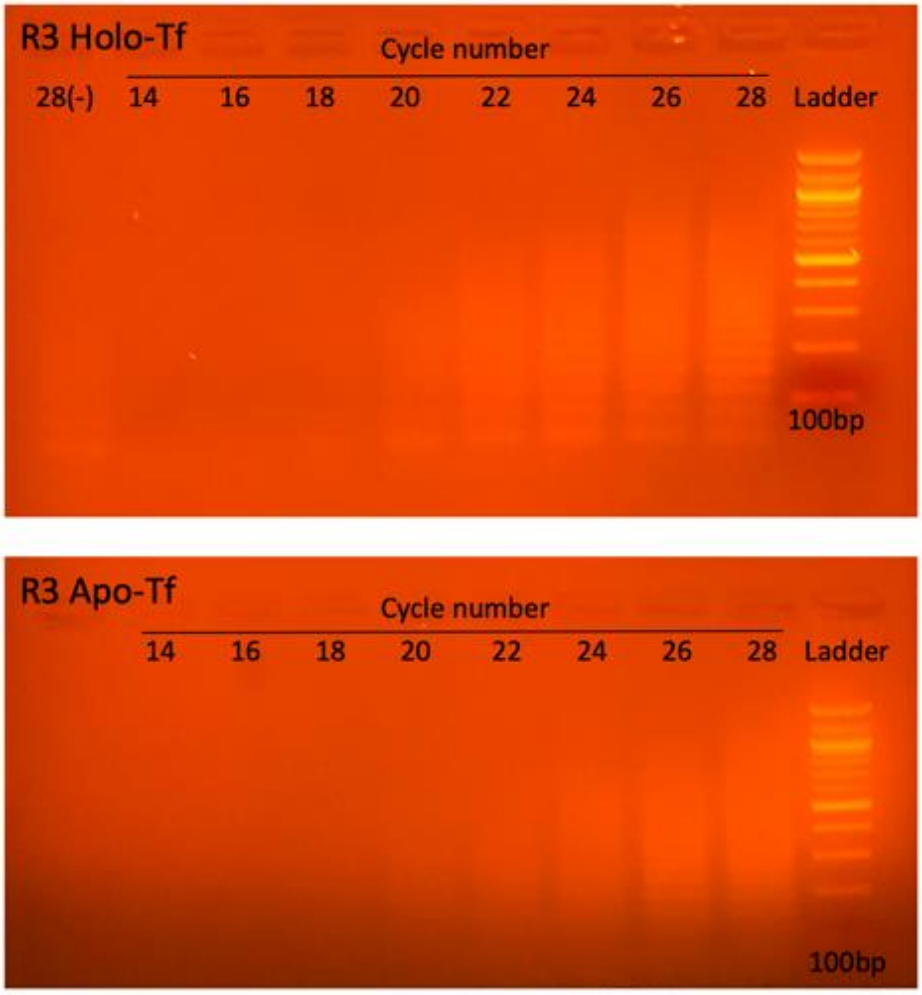

Supplemental Figure 2.11 Smearing PCR bands from R3 of the 3rd attempt of target immobilization SELEX.
The analytical PCR bands shown on gel electrophoresis for R3 holo-Tf (top) and apo-Tf (bottom). The aptamer is 80-nt long, which is expected to have a band beneath 100 bp ladder (right). Lane "28(-)" is a blank PCR control.

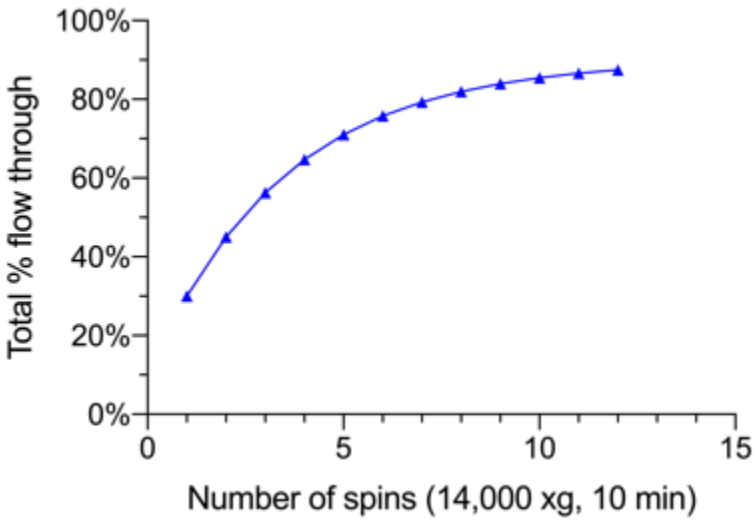

Supplemental Figure 2.12 Model of % total aptamer flow through after each spin on 100k size cutoff column.
The curve represents % total flow through as the number of spins is increasing. The model estimates 30% flows through first spin, 25% of remainder flows through in every next spin, 10% stuck in the column. The estimations were made based on tested data (not shown).

Chapter 3. CHARACTERIZATION OF TRUNCATED JURKAT BINDING APTAMER

Abstract

An 81-nt DNA aptamer termed Jurkat binding aptamer (JBA) and its 51-nt truncated form (tJBA) were previously identified by our group via cell-SELEX, during which Jurkats and J.RT3-T3.5 were used for positive and negative selection, respectively. Pull-down assay and mass spectrometry (MS) analysis have pointed to transferrin receptor (TfR, also known as CD71) as the target of the JBA and tJBA. We further support our hypothesis by short interfering RNA (siRNA) knockdown of Jurkats and bio-layer interferometry binding of CD71 recombinant protein. Furthermore, we demonstrate the cross-reactivity of tJBA in murine cells, on which the binding pocket minimally overlaps with that of holo-Tf. Co-incubation of tJBA with mCD71 Ab caused a 4-fold increase of tJBA binding on EL4, an interesting finding that can potentially be utilized to develop novel cancer cell apoptosis assays. We finally present our preliminary data in an attempt to push the results towards *in vivo* applications by improving the serum stability of tJBA and the understanding of the structure-function relationship.

3.1 INTRODUCTION

Transferrin receptor (TfR, also known as CD71) is expressed in higher abundance in rapidly dividing cells than in quiescent cells, since CD71 plays a critical role in iron uptake and rapid cell proliferation.[110] There is an elevated expression in cancer cells and on the endothelium of the BBB than in healthy cells.[111] Studies have shown that CD71 is more highly expressed in malignant tissues than their normal cell counterparts.[112,113] It is therefore a suitable target for treatment and

diagnosis of cancer as well as brain diseases such as GBM, Alzheimer's disease and other neurological disorders.

A number of studies have demonstrated therapeutic outcomes in the brain in animal models using TfR-targeting molecules for drug delivery payloads.[69,72,76,81,98] For instance, anti-TfR antibodies that do not compete with Tf for TfR binding have been developed for RMT-based delivery. OX26 antibody, which recognize rat CD71, was one of the first targeting molecule to be tested.[114] OX26 constructed with different drugs or nanoparticles showed therapeutic efficacy in preclinical models of brain disease.[115,116] This strategy is further optimized by switching to low-affinity variants after subsequent studies had shown that a high affinity binder like OX26 remained in the endothelial cells without transportation to the brain parenchyma.[69] Despite recent improvements, challenges remain to provide solutions for the systematic toxicity and the immunological risk of Abs, as well as the need to develop species-specific Abs.[98,117]

An 81-base-pair DNA aptamer that binds to Jurkats, a human T lymphocyte cell line, with a low nanomolar range affinity was previously identified by the Pun lab. The aptamer was selected via cell-SELEX, during which Jurkats and J.RT3-T3.5 were used for positive and negative selection, respectively. J.RT3 is a mutant Jurkat strain that does not express CD3, CD28 or T cell receptor on the surface.[118] This aptamer, named Jurkat binding aptamer (JBA), as well as its truncated form, 51-base-pair long tJBA (**Figure 3.1**), had shown high binding affinity towards human activated T cells, B cells and monocytes. With pull-down assay gel (**Supplemental Figure 3.11**) and mass spectrometry (MS) analysis (**Supplemental Table 3.2**), we propose that CD71 is the protein target for tJBA.

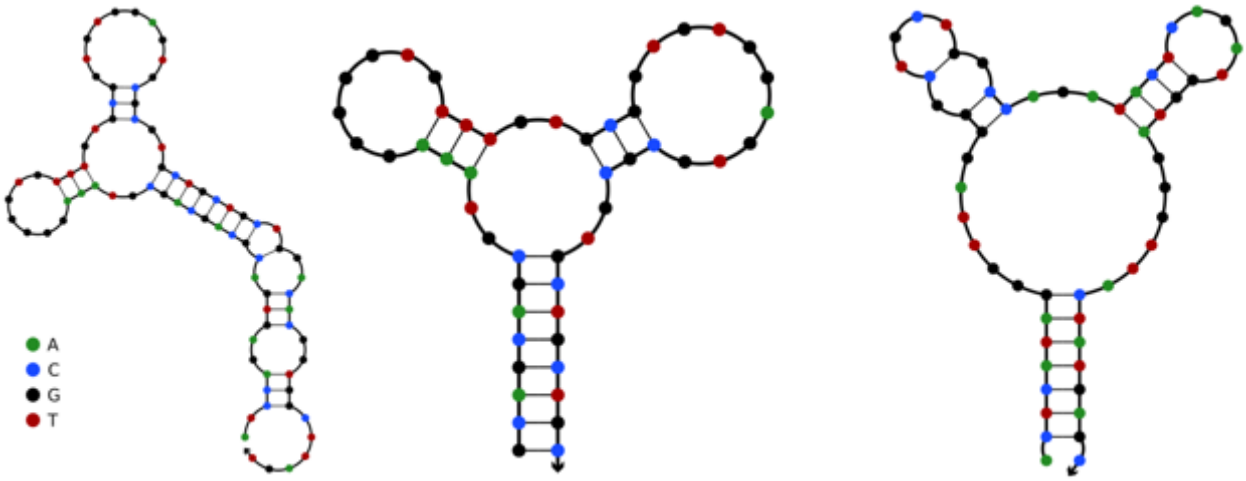

Figure 3.1 Secondary structure of JBA (left), tJBA (middle), and XQ-2d (right).
The minimum free energy secondary structures were predicted using NUPACK (temperature = 4°C; Na^+ = 137 mM; Mg^{2+} = 5.5 mM).[119] Free energy of the secondary structure were calculated to be -25.85, -18.04, and -15.24 kcal/mol for JBA, and tJBA, and XQ-2d, respectively. Specific sequences are summarized in **Supplemental Table 3.1**.

Here, we demonstrated our effort to validate CD71 as the target for tJBA and characterized the binding profile of tJBA against cells and CD71 recombinant proteins. We also compared the binding profiles of tJBA with another human CD71 targeting aptamer, XQ-2d (**Figure 3.1 right**).[120] XQ-2d is a 56 base-pair long DNA aptamer selected against pancreatic ductal adenocarcinoma (PDAC) cancer cells using human PDAC PL45 cell line and normal hTERT-HPNE as targets for positive and negative selection, respectively.[121] Furthermore, we showed the potential of tJBA to cross react between mouse and human cells. Lastly, we presented our preliminary results in improving its *in vivo* stability and in gaining deeper understanding of tJBA binding mechanism.

3.2 Material and Methods

3.2.1 *Materials*

The following dyes and antibodies used to stain cells were purchased from BioLegend: Zombie Violet (1:500 in 100 µl 10^{-6} cells), Zombie Yellow (1:500 in 100 µl 10^{-6} cells), FITC anti-mouse

CD3ε Antibody (1:50, 100305), purified anti-mouse CD71 Antibody (1:50, 113802). Samples were analyzed using an Attune NxT (Invitrogen) flow cytometer.

Buffer Components. Washing buffer (WB): DPBS, 5.5mM $MgCl_2$, 4.5 mg/ml glucose. Binding buffer (BB): WB supplemented with competitors, including 0.1 mg/ml tRNA, 0.1 mg/ml salmon sperm DNA, and different concentrations of BSA.

3.2.2 *Cell Culture and siRNA Knockdown*

Jurkat and EL4 cell lines (ATCC) were cultured in RPMI 1640 medium (Gibco) with 10% heat-inactivated FBS (Life Tech and VWR) and DMEM, high glucose (Gibco) with 10% heat-inactivated FBS (Life Tech and VWR), respectively. Jurkats were nucleofected with 30 pmol of TFRC siRNA or scrambled duplex siRNA (IDT) using the Human T Cell Nucleofector Kit (Lonza) with Program X-001 according to the manufacturer's instructions. Aptamer and anti-CD71 antibody staining were performed 22 h later and analyzed via flow cytometry.

3.2.3 *Aptamer Binding and Antibody/protein Competition Assays*

10^5 cells were incubated with 100 µl of folded FAM- or Cy5-labelled individual aptamers for 30 min at 4 °C in binding buffer at the indicated concentrations. For CD71 Ab or transferrin protein competition studies, antibodies or proteins were added at the indicated concentrations and were co-incubated with aptamer. Cells were washed twice in 200 µl of wash buffer supplemented with 1% BSA to remove excess aptamer. Stained cells were fixed in 200 µl of wash buffer with 1% BSA and 0.2% PFA before analysis via flow cytometry.

3.2.4 *Bio-Layer Interferometry (BLI).*

BLI studies were conducted on a FortéBio Octet Red96 instrument with protocol adapted from previous BLI studies. The sample buffer used for all steps were comprised of WB with 1% BSA, 0.1mg/mL yeast tRNA, and 0.01% Tween 20. Streptavidin-coated biosensors were loaded with 50 nM biotinylated aptamer. During the association step, sensors were exposed to a 1:2 dilution series of Fc-tagged human transferrin receptor recombinant protein or His-tagged murine transferrin receptor recombinant protein (Sino Biological) ranging from 400 to 50 nM. Association and dissociation steps were carried out for 1,800 s, respectively. Data analysis was carried out using Octet Data Analysis 9.0 (FortéBio).

3.2.5 *AMBER modeling*

The Vienna number of tJBA was generated from the MFOLD Web server,[122] and the corresponding three-dimensional structure with best predicted energy was constructed using the RNAcomposer software.[123] After nucleic acid bases U were changed to T, Molecular dynamics simulation (MD) was performed using the sander module implemented in the Amber 18 suite[124] with bsc1 force field. Hydrogen atoms and sodium ions (to neutralize the negative charges) were added using the *tleap* utility. The simulation system was immersed in a truncated octahedral box of TIP3P explicit water, extended 10 Å outside the aptamer on all sides. To start the MD simulation, initial structure of the aptamer was treated as follows: (a) water molecules and counter ions were relaxed to minimize energy for 10,000 minimization steps (5,000 steepest descent steps and 5,000 conjugate-gradient steps) with the DNA restrained with a force constant of 500 kcal mol^{-1} $Å^{-2}$; (b) the whole system was then minimized without restraints for 10,000 minimization steps. After energy minimization, the system was gradually heated in the NVT

ensemble from 0 to 300 K over 50 ps. This procedure was followed by 50 ps of NPT simulation at 300 K and 1 atm pressure. After that, 50 ns production MD run was performed. All processing and analysis of the MD trajectory data were performed using CPPTRAJ module.

3.3 Results and Discussion

3.3.1 *tJBA Binding to Human TfR*

One critical validation step to confirm whether hCD71 is the binding target of tJBA is via short interfering RNA (siRNA) knockdown in Jurkats. siRNA induced gene silencing is a powerful technique to knock down gene expression for the associated protein function studies.[125] We hypothesized that the reduction of binding will be similar for hCD71 antibody and tJBA on Jurkats after transferrin receptor gene 1 (*TFRC*) knockdown. XQ-2d, the hCD71 binding aptamer from literature,[120] was compared side-by-side.

There was an approx. 40% reduction of hTfR antibody staining, as well as both tJBA and XQ-2d binding after *TFRC* knockdown by siRNA in Jurkats, compared to those transfected with non-specific siRNA (**Figure 3.2**). The similar down regulation suggests that tJBA and XQ-2d bind to the same target as CD71 Ab does on cells.

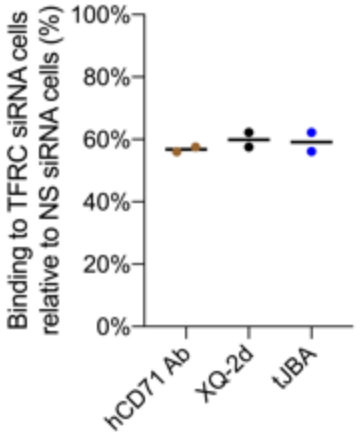

Figure 3.2 Binding of human CD71 antibody, tJBA, and XQ-2d aptamer to Jurkats after nucleofection with TFRC siRNA or non-specific siRNA.

The binding was analyzed via flow cytometry 22 h after nucleofection. TFRC siRNA data points are normalized to non-specific siRNA-treated controls (100% binding).

The binding of tJBA to TfR was further confirmed by biolayer interferometry (BLI), in which a serial dilution of recombinant hTfR was tested for association and dissociation kinetics against tJBA immobilized on streptavidin-coated BLI sensors (**Figure 3.3**). tJBA binds to TfR protein with a K_d value of 5.02 (±0.09) nM while XQ-2d binds with a K_d value of 17.9 (±0.2) nM. A small dissociation (k_{dis}) rate constant contributes to the low nanomolar range affinity of tJBA.

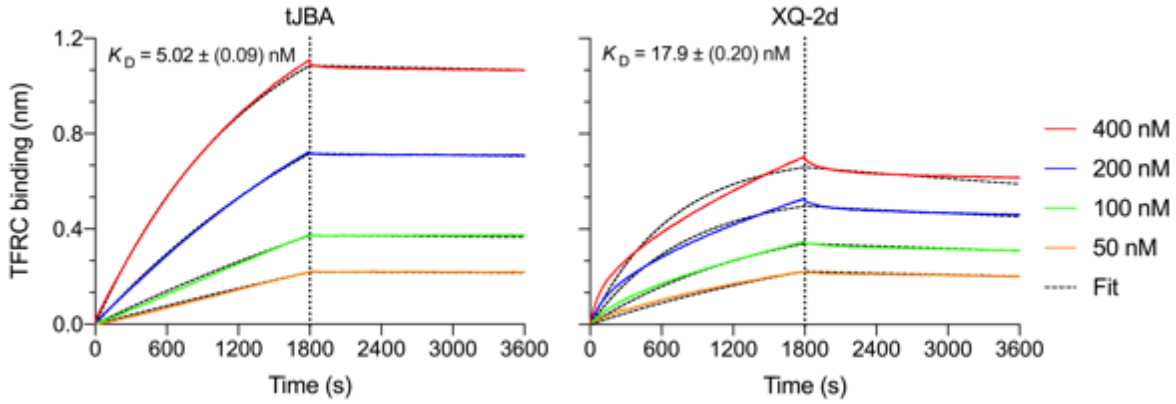

Figure 3.3 BLI-measured association and dissociation kinetics of serially diluted Fc-tagged human transferrin receptor recombinant protein (hCD71) binding to immobilized tJBA and XQ-2d aptamers.
The association phase is illustrated from 0−1,800 s, whereas dissociation is shown from 1,800–3,600 s (separated by the vertical dotted line). K_d values were calculated by performing a global fit of the kinetic data at the different concentrations of TFRC protein to a 1:1 binding model. K_d values are the mean ± s.d.; n = 4 individual concentrations for tJBA and XQ-2d, respectively.

Structural compatibility acts as a critical source for aptamer-target binding. tJBA and XQ-2d shared sequence homology and structure similarities. Both aptamers were predicted to have a stem-loop structure with two hairpins on a loop (**Figure 3.1**). XQ-2d were found to show affinity to multiple cancer cells lines, including leukemia, prostate cancer, gastric cancer, and break cancer cell lines.[121] The resemblance between the two aptamers is consistent with our findings that tJBA binds to CD71, a membrane protein that is similarly upregulated in many cancers.[77,110]

There is an approx. 4-fold increase of tJBA binding to hCD71 compared to XQ-2d. Regarding their potential for drug delivery to the brain, it is unclear if a low-nanomolar-range tight binding is more beneficial for crossing the BBB. The concern originates from the observation that OX26 Abs were found to accumulate in the BBB endothelium cells instead of penetrating the brain.[126] The extremely high-affinity (K_d = 5 nM) Ab remains bound to TfR after the vesicle fuses to the basal endothelium and prevents the release of OX26 into the brain.[126] As a result, careful considerations and design are needed to utilize the tight binding nature of tJBA at the application end.

3.3.2 *tJBA Cross Reactivity to Murine CD71*

Murine CD71 and human CD71 share approximately 77% sequence homology.[127] Since having a cross reactive aptamer is beneficial for translational research, we aimed to investigate whether tJBA possess any binding affinity towards murine transferrin receptors. We performed a binding study of tJBA on EL4, a murine lymphoblast cell line that expresses elevated levels of mCD71 on the surface. While tJBA binds to EL4 with a binding affinity of 7.71 (±3.9) nM, XQ-2d demonstrates a binding profile similar to a nonspecific aptamer control (**Figure 3.4**). tJBA maintained a low nanomolar range binding affinity to murine lymphoblast cell that express an elevated amount of mCD71 on the surface while XQ-2d did not.

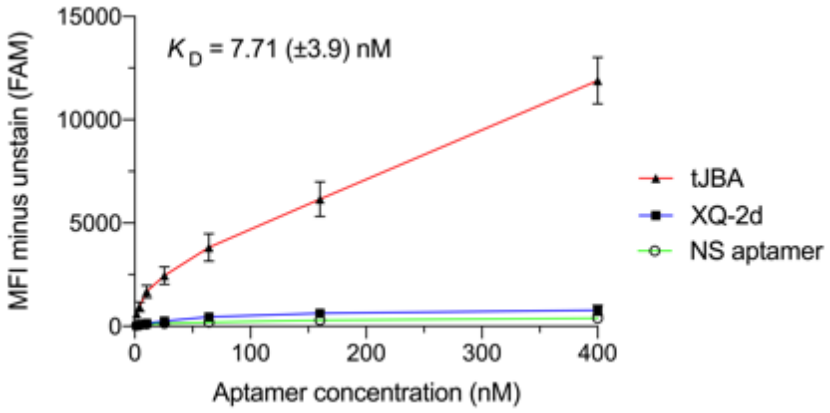

Figure 3.4 The flow cytometry binding curves of tJBA, XQ-2d, and NS aptamer to EL4 cells. The curves represent a nonlinear regression assuming one-site total binding of three independent experiments with technical triplicates. K_d values were calculated by averaging the individual regression values of the independent experiments. Data points and error bars, and K_d values, are the mean ± s.d.; n = 3 independent experiments. NS, non-specific.

Encouraged by these results, we then sought to determine the binding of tJBA to murine TfR protein itself by biolayer interferometry (BLI). A serial dilution of recombinant murine CD71 was tested for association and dissociation kinetics against tJBA immobilized on streptavidin-coated BLI sensors (**Figure 3.5**). Interestingly, the OCTET signal was inverted, which was unusual for an approx. 190 kDa protein. While a nonspecific aptamer negative control showed no detectable signal change, tJBA exhibited signal change with a concentration dependent manner with the His-tagged mCD71 protein. It was therefore no possible to calculate the dissociate constant K_d. After multiple troubleshooting attempts, such as elevated concentration of blocking agents in buffer, incubation of protein with reducing agent (**Supplemental Figure 3.12**), and repeating experiment on new batch of protein all rendered unsuccessful, we speculate the cause was associated with the intrinsic property of mCD71.

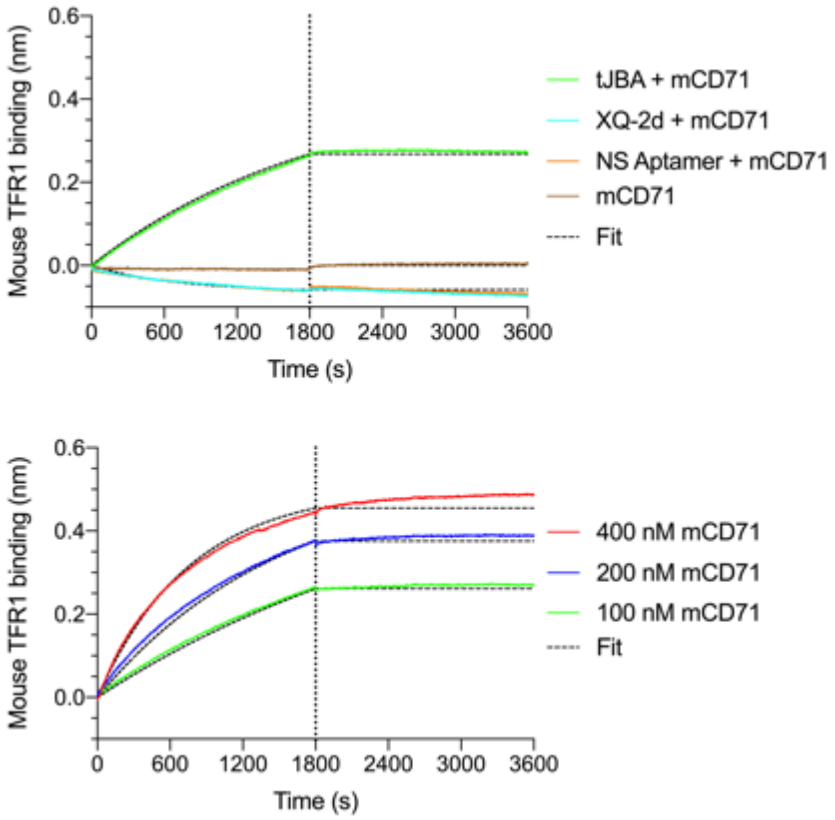

Figure 3.5 BLI-measured association and dissociation kinetics of His-tagged murine transferrin receptor recombinant protein (mCD71) binding to immobilized tJBA, XQ-2d, and NS aptamer. Aptamers concentrations are kept at 50 nM. Binding signals are flipped. On the left shows 100 nM mCD71 binding to immobilized tJBA, XQ-2d, and NS aptamers; on the right shows serially diluted mCD71 binding to immobilized tJBA. The association phase is illustrated from 0−1,800 s, whereas dissociation is shown from 1,800–3,600 s (separated by the vertical dotted line).

To have a better understanding in the binding pocket of tJBA on mCD71, a competition assay was performed for tJBA to murine EL4 cells against different fold excesses of endogenous holo-transferrin recombinant protein, the natural ligand of TfR. While 1:1 ratio competes off 20% of tJBA binding, 32X fold excess of murine Tf competes off 80% of tJBA binding (**Figure 3.6**). The results suggest that either (1) tJBA does not share the entirely same binding pocket as holo-Tf in the extracellular region of mCD71. The binding of tJBA interferes with endogenous murine holo-Tf binding to a limited extent; or (2) tJBA and Tf have a similar binding pocket but with

different affinities; or (3) other target(s) of tJBA exist on the cell surface of EL4; or (4) tJBA binds EL4 with a non-specific component.

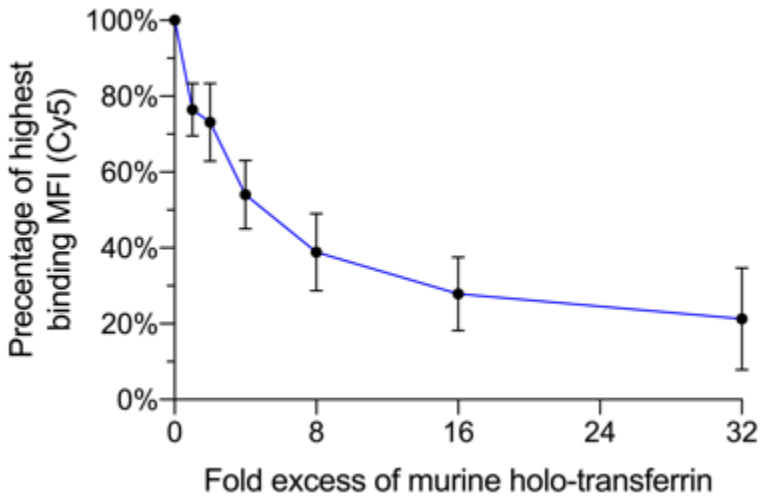

Figure 3.6 The flow cytometry binding curve of tJBA to murine EL4 cells in competition of serially diluted murine holo-transferrin recombinant protein.
Concentrations of aptamer are kept at 25 nM, while concentrations of protein ranges from 1X to 32X above that of aptamer. Data points and error bars are the mean ± s.d.; n = 3 independent experiments.

Another competition assay was performed on tJBA to assess the binding site compared to murine anti-mCD71 antibody. Concentrations of antibody ranging from 16X below to 8X above that of tJBA were incubated with EL4 cells. Interestingly, there was a 4-fold increase of tJBA binding in the presence of murine antibody (**Figure 3.7**). Instead of abrogating aptamer binding, antibody has a stabilization effect on tJBA binding to EL4 cells.

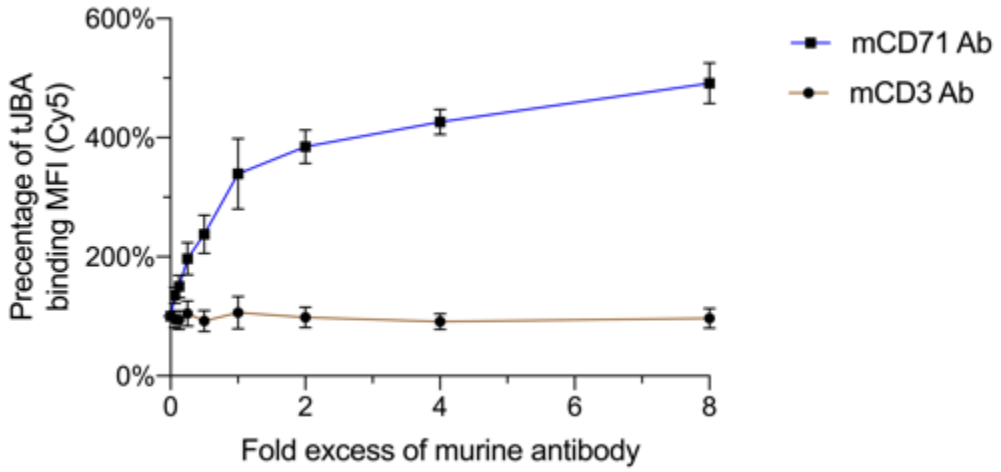

Figure 3.7 The flow cytometry binding curves of tJBA to murine EL4 cells in competition of serially diluted mCD71 antibody and mCD3ε antibody.
Concentrations of aptamer are kept at 25 nM, while concentrations of proteins ranges from 16X below to 8X above that of aptamer. Data points and error bars are mean ± s.d.; n = 3 independent experiments.

The results above demonstrates the cross reactivity of tJBA between human and murine CD71. Cross reactivity is a favorable trait compared to species-specific Abs for further translational work at the application end. A significant barrier for taking a step forward from bench-top research to clinical trials is the lack of efficient characterization of the therapy *in vivo*. The problem arises when the true efficacy of the developed therapeutics cannot be faithfully reflected using animal models. Therefore, the cross reactivity of tJBA is a highly attractive trait for future functionalization and therapeutic applications.

Competition studies yielded interesting insights into the binding profiles of tJBA on mCD71. Murine CD71 antibody has a synergistic effect and cause a 4-fold increase of tJBA binding when co-incubated with EL4. Since CD71 is the main receptor responsible for the cell iron supply, its expression is closely related to the proliferation of cells.[128] Iron deprivation has emerged to be a new strategy for cancer therapeutics due to the high iron content tumors have and their dependence on iron for growth and progression. Previous studies have reported the decrease of cell viability in cancer cell lines after incubation with CD71 monoclonal

antibodies.[129,130] The reduction could be due to the mCD71 Ab competing with the iron bearing natural ligand holo-Tf, inhibiting CD71 internalization, or inducing CD71 degradation.[130] The increased binding of tJBA with mCD71 Ab opens up potential applications for enhanced inhibition effect on cell proliferation.

3.4 Preliminary Results for Future Perspectives

With an exponentially increasing number of related publications, the aptamer field has witnessed the creation and development of a wide range of aptamers with various targets and specificities. However, the utility of aptamers in research, diagnostic, and therapeutic applications has been constrained by the limited metabolic stability of nucleic acids. Moreover, in the case of tJBA, a more comprehensive understanding of the binding mechanism is critical in pushing the current results towards the application end. In other words, more information about the structure−function relationship is crucial in helping to explain the cross-reactivity of tJBA in mice (**Figure 3.4**) and the stabilization effect of mCD71 Ab on tJBA with EL4 (**Figure 3.7**).

3.4.1 *Modification of tJBA with LNA 2'OMe*

The relatively simple chemical structure of aptamers has allowed the insertion of fluorescent reporter molecules as well as modifications in specific locations on the oligonucleotide. In attempt to improve the thermal stability and resistance against nucleolytic degradation of tJBA *in vivo*, LNA (Locked Nucleic Acid) building blocks and 2'OMe modifications were added to the tJBA structure (**Figure 3.8**).

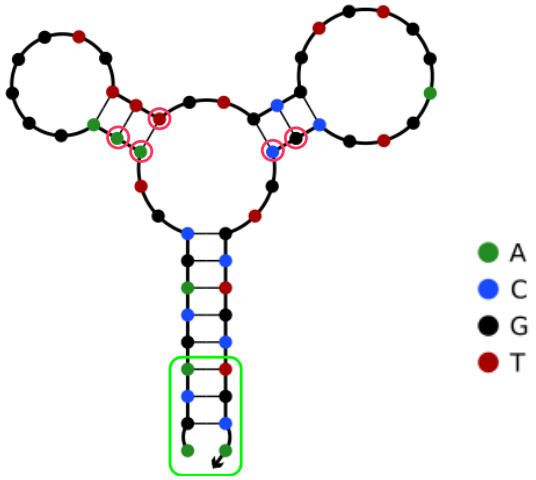

Figure 3.8 Secondary structure of LNA-2'OMe-tJBA.
The minimum free energy secondary structures were predicted using NUPACK (temperature = 4°C; Na^+ = 137 mM; Mg^{2+} = 5.5 mM).[119] Individual nucleotides with LNA modifications were circled in red; Nucleotides with 2'OMe modifications were squared in green. The specific sequence is listed in **Supplemental Table 3.1**.

The binding of LNA-2'OMe modified tJBA to Jurkat cells were compared to unmodified tJBA at two different temperatures (**Figure 3.9**). The binding affinities were calculated to be 64.37 nM and 245.3 nM for LNA-2'OMe tJBA, 16.06 nM and 54.06 nM for unmodified tJBA at 4°C and 37°C, respectively. There was a similar fold decrease (3.8 vs. 3.4) of binding due to temperature change for both modified and unmodified tJBA, suggesting that binding stability was not benefited from the added modifications; The affinity decreased by 4-fold after modifications at both temperatures, suggesting that LNA and 2'OMe nucleotides were not well-tolerated in the structure, which reflected their critical roles in binding of the oligonucleotide. Previous studies have suggested that single substitutions in the stem regions of aptamers showed increased binding affinities compared to unmodified ones.[131] It is possible that having multiple LNA-containing nucleotides at the stem of the hairpins is too constrained to confer the appropriate binding conformation of the aptamer. The impact of these alterations needs further assessment before further *in vivo* applications.

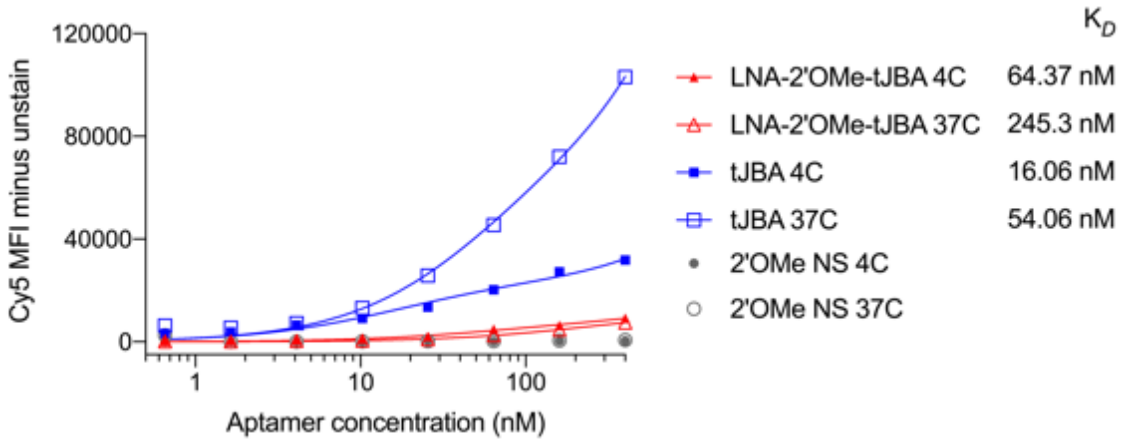

Figure 3.9 The flow cytometry binding curves of LNA-2'Ome-tJBA, tJBA, and nonspecific (NS) aptamer to Jurkats.
The curves represent a nonlinear regression assuming one-site total binding. The equilibrium dissociation constant K_d for the aptamer binding affinity was calculated by the equation Y = Bmax * X/ (K_d + X) + NS * X. Bmax, the maximum specific binding; NS, the slope of non-specific binding.

3.4.2 *3D Structure of tJBA Predicted by AMBER19*

The first step towards having a better understanding of the molecular level interactions among tJBA, mCD71, and mCD71 Ab is to predict the 3D structure of aptamer. Starting with the nucleotide sequences, the secondary structure of tJBA was predicted using the Mfold web server[122] based on free energy minimization techniques. Using the RNAcomposer software,[123] the Vienna number of tJBA outputted by Mfold was used to generate the initial input structure for AMBER molecular dynamics (MD).[124] After manually changing all Us to Ts, the structure was neutralized and solvated to generate the input files to run MD using sander. A 50 ns production MD run was performed to generate the 3D structure of tJBA (**Figure 3.10**). The structure is consistent with the secondary predicted by NUPACK (**Figure 3.1 middle**). The 3D structure of tJBA lays the foundation for future docking analysis between tJBA and CD71, as well as its interaction with holo-Tf and antibody to explain the binding behavior of tJBA.

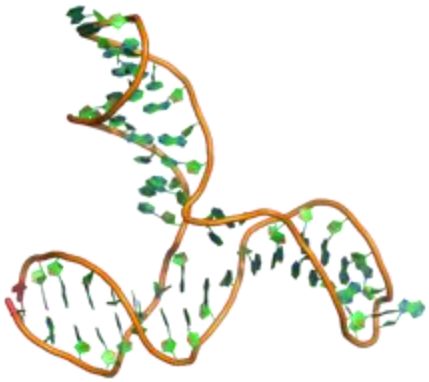

Figure 3.10 3D structure of tJBA predicted by AMBER19.
The minimum free energy 3D structure of tJBA was predicted using AMBER19.[124] A 50 ns molecular dynamics simulation was performed to eliminate the steric conflicts within the aptamer system.

3.5 CONCLUSIONS

Here, we provided further analysis to support the hypothesis that CD71 protein present on the cell surface is the binding target of tJBA. tJBA binds to hCD71 protein with K_d value of 5.02 (±0.09) nM, approx. 4-fold better than XQ-2d, a hCD71 aptamer from literature with K_d of 17.9 (±0.2) nM. Moreover, we demonstrated the cross-reactivity of tJBA, but not XQ-2d, in human and murine cancer cells. The binding of tJBA on mCD71-expressing cells did not entirely compete off holo-Tf binding, suggesting the two binding pockets have limited overlap. Co-incubation of tJBA with mCD71 Ab caused a 4-fold increase of tJBA binding on EL4. This synergy could potentially be utilized to develop cancer cell apoptosis assays for novel strategies of therapeutics. tJBA with LNA and 2'OMe modifications lost targeting affinity by 4-fold, suggesting that nucleotides at the stem of the hairpins play critical roles in conferring the appropriate binding conformation of the aptamer. Finally, AMBER MD simulation revealed the 3D structure of tJBA, setting the foundation for obtaining a more comprehensive of tJBA binding profiles via in silico methodology.

3.6 SUPPLEMENTAL INFORMATION

Supplemental Table 3.1 Sequences of JBA, tJBA, LNA-2'OMe-tJBA, and XQ-2d. "m" represents 2'OMe modification; "+" represents LNA modification.

Name	Length (nt)	Sequence
JBA	81	ATCCAGAGTGACGCAGCAGCGTAAAGGGGGTGTTTGTGCGGTGTGGAGTGCGCGTGCTGCTGCTGGACACGGTGGCTTAGT
tJBA	51	GCAGCAGCGTAAAGGGGGTGTTTGTGCGGTGTGGAGTGCGCGTGCTGCTGC
LNA-2'OMe-tJBA	53	mAmGmCmAGCAGCGT+A+AAGGGGGTGTT+TGTGCGGTGTGGAGTG+C+GCGTGCTGCmTmGmCmA
XQ-2d	56	ACTCATAGGGTTAGGGGCTGCTGGCCAGATACTCAGATGGTAGGGTTACTATGAGC

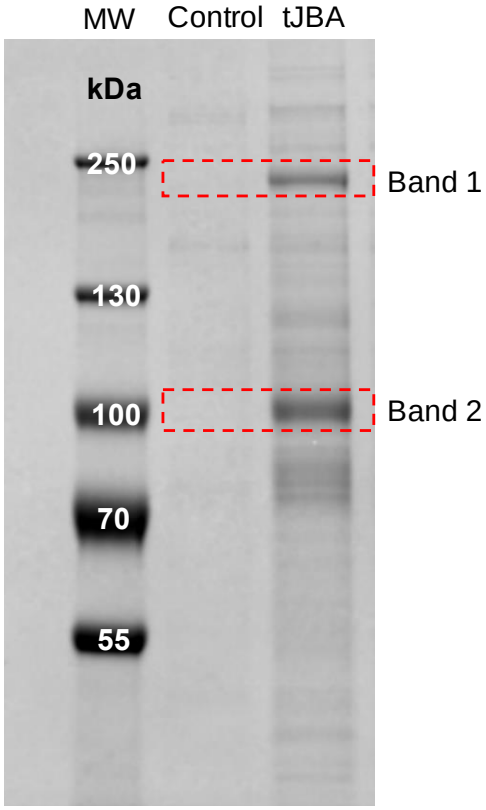

Supplemental Figure 3.11 Pull-down assay gel of tJBA with membrane protein extracted from Jurkats.

Lane 1: Biotin-saturated strep-beads (negative control); Lane 2: tJBA strep-beads (Courtesy of Emmeline Cheng).

Supplemental Table 3.2 Mass Spectrometry analysis of band 1 and 2 from pull down assay. Accessions with high FDR confidence were considered and Keratin were excluded. Top 15 scores from each band were listed (Courtesy of Emmeline Cheng).

Band	Accession	Description	Score tJBA	Score control	#peptides tJBA	#peptides control
1	P02786	Transferrin receptor protein 1	1972.92	25.26	52	4
1	P46940	Ras GTPase-activating-like protein IQGAP1	458.65	47.22	56	10
1	Q92608	Dedicator of cytokinesis protein 2	443.53	27.5	62	9
1	Q92614	Unconventional myosin-XVIIIa	155.65	27.15	32	7
1	Q6WKZ4	Rab11 family-interacting protein 1	101.76	35.76	20	8
1	P26358	DNA (cytosine-5)-methyltransferase 1	98	3	23	1
1	Q9ULH0	Kinase D-interacting substrate of 220 kDa	90.2	0	21	0
1	A0A087WUT6	Eukaryotic translation initiation factor 5B	71.33	29.52	17	6
1	Q5SXM2	snRNA-activating protein complex subunit 4	56.14	0	14	0
1	R4GMW8	BIVM-ERCC5 readthrough	53.68	0	10	0
1	Q14004	Cyclin-dependent kinase 13	53.51	0	13	0
1	P08575	Receptor-type tyrosine-protein phosphatase C	49.99	0	14	0
1	O75093	Slit homolog 1 protein	47.83	20	11	4
1	P49815	Tuberin	47.8	0	12	0
1	Q9C0C9	(E3-independent) E2 ubiquitin-conjugating enzyme	42.36	2.81	11	1
2	P02786	Transferrin receptor protein 1	2283.59	17.66	50	5
2	P33992	DNA replication licensing factor MCM5	262.49	21.37	39	4

2	H7BXI1	Extended synaptotagmin-2 (Fragment)	206.06	27.56	25	7
2	O43143	Pre-mRNA-splicing factor ATP-dependent RNA helicase DHX15	138.5	9.52	22	3
2	O94874	E3 UFM1-protein ligase 1	135.23	32.35	22	7
2	Q16891	MICOS complex subunit MIC60	119.12	12.07	26	5
2	P08238	Heat shock protein HSP 90-beta	113.87	20.36	18	4
2	A0A0U1RRB6	Exocyst complex component	89.86	11.19	16	2
2	Q12906	Interleukin enhancer-binding factor 3	85.87	4.62	17	1
2	Q9UGP8	Translocation protein SEC63 homolog	81	2.23	15	1
2	P50416	Carnitine O-palmitoyltransferase 1, liver isoform	78.13	9.7	18	2
2	P07900	Heat shock protein HSP 90-alpha	76.35	17.84	14	4
2	Q13724	Mannosyl-oligosaccharide glucosidase	71.74	2.5	13	1
2	Q8TAG9	Exocyst complex component 6	69.9	2.12	14	2
2	Q14974	Importin subunit beta-1	65.82	3.46	12	1

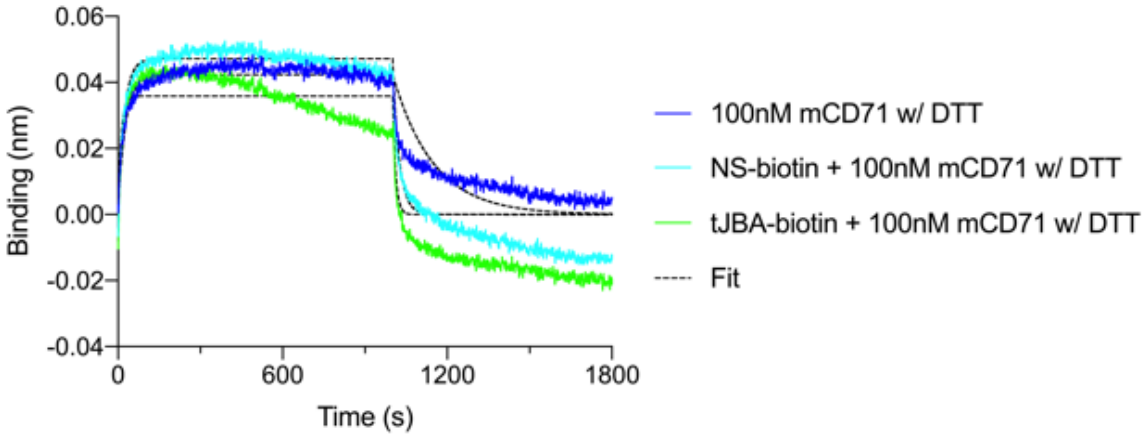

Supplemental Figure 3.12 BLI-measured association and dissociation kinetics of DTT-treated His-tagged mCD71 recombinant protein binding to immobilized tJBA.
The association phase is illustrated from 0−1,000 s, whereas dissociation is shown from 1,000–1,800 s.

BIBLIOGRAPHY

1 Ellington, A. D. & Szostak, J. W. In vitro selection of RNA molecules that bind specific ligands. *Nature* **346**, 818-822, doi:10.1038/346818a0 (1990).

2 Tuerk, C. & Gold, L. Systematic evolution of ligands by exponential enrichment: RNA ligands to bacteriophage T4 DNA polymerase. *Science* **249**, 505-510, doi:10.1126/science.2200121 (1990).

3 Famulok, M., Hartig, J. S. & Mayer, G. Functional Aptamers and Aptazymes in Biotechnology, Diagnostics, and Therapy. *Chemical Reviews* **107**, 3715-3743, doi:10.1021/cr0306743 (2007).

4 Nimjee, S. M., White, R. R., Becker, R. C. & Sullenger, B. A. Aptamers as Therapeutics. *Annu Rev Pharmacol Toxicol* **57**, 61-79, doi:10.1146/annurev-pharmtox-010716-104558 (2017).

5 Ashrafuzzaman, M. Aptamers as both drugs and drug-carriers. *BioMed research international* **2014** (2014).

6 Darmostuk, M., Rimpelova, S., Gbelcova, H. & Ruml, T. Current approaches in SELEX: An update to aptamer selection technology. *Biotechnol Adv* **33**, 1141-1161, doi:10.1016/j.biotechadv.2015.02.008 (2015).

7 Dunn, M. R., Jimenez, R. M. & Chaput, J. C. Analysis of aptamer discovery and technology. *Nature Reviews Chemistry* **1**, 0076, doi:10.1038/s41570-017-0076 (2017).

8 Brody, E. N. *et al.* The use of aptamers in large arrays for molecular diagnostics. *Molecular Diagnosis* **4**, 381-388 (1999).

9 Haller, A., Altman, R. B., Soulière, M. F., Blanchard, S. C. & Micura, R. Folding and ligand recognition of the TPP riboswitch aptamer at single-molecule resolution. *Proceedings of the National Academy of Sciences* **110**, 4188-4193 (2013).

10 Shaw, J. P., Kent, K., Bird, J., Fishback, J. & Froehler, B. Modified deoxyoligonucleotides stable to exonuclease degradation in serum. *Nucleic Acids Res* **19**, 747-750, doi:10.1093/nar/19.4.747 (1991).

11 Lipi, F., Chen, S., Chakravarthy, M., Rakesh, S. & Veedu, R. N. In vitro evolution of chemically-modified nucleic acid aptamers: Pros and cons, and comprehensive selection strategies. *RNA Biol* **13**, 1232-1245, doi:10.1080/15476286.2016.1236173 (2016).

12 Breslow, R. & Chapman, W. H. On the mechanism of action of ribonuclease A: relevance of enzymatic studies with a p-nitrophenylphosphate ester and a thiophosphate ester. *Proceedings of the National Academy of Sciences* **93**, 10018-10021 (1996).

13 Ng, E. W. *et al.* Pegaptanib, a targeted anti-VEGF aptamer for ocular vascular disease. *Nature reviews drug discovery* **5**, 123-132 (2006).

14 Lietard, J. *et al.* Mapping the affinity landscape of Thrombin-binding aptamers on 2′ F-ANA/DNA chimeric G-Quadruplex microarrays. *Nucleic acids research* **45**, 1619-1632 (2017).

15 Wilds, C. J. & Damha, M. J. 2′-Deoxy-2′-fluoro-β-D-arabinonucleosides and oligonucleotides (2′ F-ANA): synthesis and physicochemical studies. *Nucleic acids research* **28**, 3625-3635 (2000).

16 Singh, S. K., Koshkin, A. A., Wengel, J. & Nielsen, P. LNA (locked nucleic acids): synthesis and high-affinity nucleic acid recognition. *Chemical communications*, 455-456 (1998).

17 Glud, S. Z. *et al.* Naked siLNA-mediated gene silencing of lung bronchoepithelium EGFP expression after intravenous administration. *Oligonucleotides* **19**, 163-168 (2009).
18 Röthlisberger, P. & Hollenstein, M. Aptamer chemistry. *Advanced Drug Delivery Reviews* **134**, 3-21, doi:https://doi.org/10.1016/j.addr.2018.04.007 (2018).
19 Ismail, S. I. & Alshaer, W. Therapeutic aptamers in discovery, preclinical and clinical stages. *Advanced drug delivery reviews* **134**, 51-64 (2018).
20 Sundberg, E. J. *et al.* Estimation of the hydrophobic effect in an antigen− antibody protein− protein interface. *Biochemistry* **39**, 15375-15387 (2000).
21 Gold, L. *et al.* Aptamer-based multiplexed proteomic technology for biomarker discovery. *Nature Precedings*, 1-1 (2010).
22 Balintová, J. *et al.* Carborane-linked 2′-deoxyuridine 5′-O-triphosphate as building block for polymerase synthesis of carborane-modified DNA. *Bioorganic & medicinal chemistry letters* **27**, 4786-4788 (2017).
23 Verga, D., Welter, M., Steck, A.-L. & Marx, A. DNA polymerase-catalyzed incorporation of nucleotides modified with a G-quadruplex-derived DNAzyme. *Chemical Communications* **51**, 7379-7381 (2015).
24 Welter, M., Verga, D. & Marx, A. Sequence-Specific Incorporation of Enzyme–Nucleotide Chimera by DNA Polymerases. *Angewandte Chemie International Edition* **55**, 10131-10135 (2016).
25 Davies, D. R. *et al.* Unique motifs and hydrophobic interactions shape the binding of modified DNA ligands to protein targets. *Proceedings of the National Academy of Sciences* **109**, 19971-19976 (2012).
26 Gawande, B. N. *et al.* Selection of DNA aptamers with two modified bases. *Proceedings of the National Academy of Sciences* **114**, 2898-2903 (2017).
27 Iannitti, T., Cesar Morales-Medina, J. & Palmieri, B. Phosphorothioate oligonucleotides: effectiveness and toxicity. *Current drug targets* **15**, 663-673 (2014).
28 Abeydeera, N. D. *et al.* Evoking picomolar binding in RNA by a single phosphorodithioate linkage. *Nucleic acids research* **44**, 8052-8064 (2016).
29 Vater, A. & Klussmann, S. Turning mirror-image oligonucleotides into drugs: the evolution of Spiegelmer® therapeutics. *Drug discovery today* **20**, 147-155 (2015).
30 Purschke, W. G. *et al.* Identification and characterization of a mirror-image oligonucleotide that binds and neutralizes sphingosine 1-phosphate, a central mediator of angiogenesis. *Biochemical Journal* **462**, 153-162 (2014).
31 Fox, M. E., Szoka, F. C. & Fréchet, J. M. Soluble polymer carriers for the treatment of cancer: the importance of molecular architecture. *Accounts of chemical research* **42**, 1141-1151 (2009).
32 Wang, L. *et al.* Bispecific aptamer induced artificial protein-pairing: A strategy for selective inhibition of receptor function. *Journal of the American Chemical Society* **141**, 12673-12681 (2019).
33 Lee, C. H. *et al.* Pharmacokinetics of a cholesterol-conjugated aptamer against the hepatitis C virus (HCV) NS5B protein. *Molecular Therapy-Nucleic Acids* **4**, e254 (2015).
34 Xiang, D. *et al.* Superior performance of aptamer in tumor penetration over antibody: implication of aptamer-based theranostics in solid tumors. *Theranostics* **5**, 1083 (2015).
35 Wan, L.-Y. *et al.* An exploration of aptamer internalization mechanisms and their applications in drug delivery. *Expert opinion on drug delivery* **16**, 207-218 (2019).

36 Senapati, S., Mahanta, A. K., Kumar, S. & Maiti, P. Controlled drug delivery vehicles for cancer treatment and their performance. *Signal transduction and targeted therapy* **3**, 1-19 (2018).
37 Agrawal, S., Joshi, M. & Christoforidis, J. B. Vitreous inflammation associated with intravitreal anti-VEGF pharmacotherapy. *Mediators of inflammation* **2013** (2013).
38 Burdick, A. D. *et al.* Sequence motifs associated with hepatotoxicity of locked nucleic acid—modified antisense oligonucleotides. *Nucleic acids research* **42**, 4882-4891 (2014).
39 Lee, Y., Urban, J. H., Xu, L., Sullenger, B. A. & Lee, J. 2′ Fluoro modification differentially modulates the ability of RNAs to activate pattern recognition receptors. *Nucleic acid therapeutics* **26**, 173-182 (2016).
40 Chang, Y.-C. *et al.* Identification and characterization of oligonucleotides that inhibit Toll-like receptor 2-associated immune responses. *The FASEB Journal* **23**, 3078-3088 (2009).
41 Mosing, R. K. & Bowser, M. T. Isolating aptamers using capillary electrophoresis-SELEX (CE-SELEX). *Methods Mol Biol* **535**, 33-43, doi:10.1007/978-1-59745-557-2_3 (2009).
42 Cheng, C., Chen, Y. H., Lennox, K. A., Behlke, M. A. & Davidson, B. L. In vivo SELEX for Identification of Brain-penetrating Aptamers. *Molecular Therapy-Nucleic Acids* **2**, e67 (2013).
43 Miyachi, Y., Shimizu, N., Ogino, C. & Kondo, A. Selection of DNA aptamers using atomic force microscopy. *Nucleic Acids Res* **38**, e21, doi:10.1093/nar/gkp1101 (2010).
44 Wang, T., Chen, C., Larcher, L. M., Barrero, R. A. & Veedu, R. N. Three decades of nucleic acid aptamer technologies: Lessons learned, progress and opportunities on aptamer development. *Biotechnology Advances* **37**, 28-50, doi:https://doi.org/10.1016/j.biotechadv.2018.11.001 (2019).
45 Velez, T. E. *et al.* Systematic evaluation of the dependence of deoxyribozyme catalysis on random region length. *ACS Comb Sci* **14**, 680-687, doi:10.1021/co300111f (2012).
46 Sefah, K., Shangguan, D., Xiong, X., O'donoghue, M. B. & Tan, W. Development of DNA aptamers using Cell-SELEX. *Nature protocols* **5**, 1169 (2010).
47 Chen, M. *et al.* Development of cell-SELEX technology and its application in cancer diagnosis and therapy. *International journal of molecular sciences* **17**, 2079 (2016).
48 Svobodová, M., Pinto, A., Nadal, P. & O'Sullivan, C. Comparison of different methods for generation of single-stranded DNA for SELEX processes. *Analytical and bioanalytical chemistry* **404**, 835-842 (2012).
49 Mallikaratchy, P. *et al.* Aptamer directly evolved from live cells recognizes membrane bound immunoglobin heavy mu chain in Burkitt's lymphoma cells. *Molecular & Cellular Proteomics* **6**, 2230-2238 (2007).
50 Van Simaeys, D. *et al.* Identification of cell membrane protein stress-induced phosphoprotein 1 as a potential ovarian cancer biomarker using aptamers selected by cell systematic evolution of ligands by exponential enrichment. *Analytical chemistry* **86**, 4521-4527 (2014).
51 Wang, K., Fan, D., Liu, Y. & Wang, E. Highly sensitive and specific colorimetric detection of cancer cells via dual-aptamer target binding strategy. *Biosensors and Bioelectronics* **73**, 1-6 (2015).

52 Ye, X. *et al.* Iodide-Responsive Cu–Au Nanoparticle-Based Colorimetric Platform for Ultrasensitive Detection of Target Cancer Cells. *Analytical Chemistry* **87**, 7141-7147, doi:10.1021/acs.analchem.5b00943 (2015).
53 Campos, S. *et al.* Brain metastasis from an unknown primary, or primary brain tumour? A diagnostic dilemma. *Curr Oncol* **16**, 62-66 (2009).
54 Ostrom, Q. T. *et al.* CBTRUS Statistical Report: Primary Brain and Other Central Nervous System Tumors Diagnosed in the United States in 2011-2015. *Neuro Oncol* **20**, iv1-iv86, doi:10.1093/neuonc/noy131 (2018).
55 Brennan, C. W. *et al.* The somatic genomic landscape of glioblastoma. *Cell* **155**, 462-477, doi:10.1016/j.cell.2013.09.034 (2013).
56 Friedmann-Morvinski, D. Glioblastoma heterogeneity and cancer cell plasticity. *Critical Reviews™ in Oncogenesis* **19** (2014).
57 Huang, J. *et al.* Immune Checkpoint in Glioblastoma: Promising and Challenging. *Front Pharmacol* **8**, 242, doi:10.3389/fphar.2017.00242 (2017).
58 Steeg, P. S., Camphausen, K. A. & Smith, Q. R. Brain metastases as preventive and therapeutic targets. *Nat Rev Cancer* **11**, 352-363, doi:10.1038/nrc3053 (2011).
59 Achrol, A. S. *et al.* Brain metastases. *Nature Reviews Disease Primers* **5**, 5, doi:10.1038/s41572-018-0055-y (2019).
60 Gilbert, M. R. *et al.* A randomized trial of bevacizumab for newly diagnosed glioblastoma. *N Engl J Med* **370**, 699-708, doi:10.1056/NEJMoa1308573 (2014).
61 Shergalis, A., Bankhead, A., Luesakul, U., Muangsin, N. & Neamati, N. Current challenges and opportunities in treating glioblastoma. *Pharmacological reviews* **70**, 412-445 (2018).
62 Aldape, K. *et al.* Challenges to curing primary brain tumours. *Nature Reviews Clinical Oncology* **16**, 509-520 (2019).
63 Abbott, N. J., Patabendige, A. A., Dolman, D. E., Yusof, S. R. & Begley, D. J. Structure and function of the blood-brain barrier. *Neurobiol Dis* **37**, 13-25, doi:10.1016/j.nbd.2009.07.030 (2010).
64 van Tellingen, O. *et al.* Overcoming the blood-brain tumor barrier for effective glioblastoma treatment. *Drug Resist Updat* **19**, 1-12, doi:10.1016/j.drup.2015.02.002 (2015).
65 Bernacki, J., Dobrowolska, A., Nierwinska, K. & Malecki, A. Physiology and pharmacological role of the blood-brain barrier. *Pharmacol Rep* **60**, 600-622 (2008).
66 Huber, J. D., Egleton, R. D. & Davis, T. P. Molecular physiology and pathophysiology of tight junctions in the blood-brain barrier. *Trends Neurosci* **24**, 719-725, doi:10.1016/s0166-2236(00)02004-x (2001).
67 Daneman, R. The blood-brain barrier in health and disease. *Ann Neurol* **72**, 648-672, doi:10.1002/ana.23648 (2012).
68 Cioni, C., Turlizzi, E., Zanelli, U., Oliveri, G. & Annunziata, P. Expression of Tight Junction and Drug Efflux Transporter Proteins in an in vitro Model of Human Blood-Brain Barrier. *Front Psychiatry* **3**, 47, doi:10.3389/fpsyt.2012.00047 (2012).
69 Freskgard, P. O. & Urich, E. Antibody therapies in CNS diseases. *Neuropharmacology* **120**, 38-55, doi:10.1016/j.neuropharm.2016.03.014 (2017).
70 Macdonald, J., Mandarano, G., Veedu, R. N. & Shigdar, S. Development of transferrin receptor aptamers as drug delivery vehicles for the treatment of brain metastases. *Aptamers* **2**, 15-27 (2018).

71 Abbott, N. J. Blood–brain barrier structure and function and the challenges for CNS drug delivery. *Journal of inherited metabolic disease* **36**, 437-449 (2013).
72 Sharma, G. *et al.* Advances in nanocarriers enabled brain targeted drug delivery across blood brain barrier. *Int J Pharm* **559**, 360-372, doi:10.1016/j.ijpharm.2019.01.056 (2019).
73 Pulgar, V. M. Transcytosis to Cross the Blood Brain Barrier, New Advancements and Challenges. *Frontiers in Neuroscience* **12**, doi:10.3389/fnins.2018.01019 (2019).
74 Pardridge, W. M. Drug transport across the blood–brain barrier. *Journal of cerebral blood flow & metabolism* **32**, 1959-1972 (2012).
75 Salameh, T. S. & Banks, W. A. Delivery of therapeutic peptides and proteins to the CNS. *Adv Pharmacol* **71**, 277-299, doi:10.1016/bs.apha.2014.06.004 (2014).
76 Descamps, L., Dehouck, M. P., Torpier, G. & Cecchelli, R. Receptor-mediated transcytosis of transferrin through blood-brain barrier endothelial cells. *Am J Physiol* **270**, H1149-1158, doi:10.1152/ajpheart.1996.270.4.H1149 (1996).
77 Lajoie, J. M. & Shusta, E. V. Targeting receptor-mediated transport for delivery of biologics across the blood-brain barrier. *Annu Rev Pharmacol Toxicol* **55**, 613-631, doi:10.1146/annurev-pharmtox-010814-124852 (2015).
78 Dehouck, B. *et al.* A new function for the LDL receptor: transcytosis of LDL across the blood-brain barrier. *J Cell Biol* **138**, 877-889, doi:10.1083/jcb.138.4.877 (1997).
79 Lockman, P. R., Koziara, J. M., Mumper, R. J. & Allen, D. D. Nanoparticle surface charges alter blood–brain barrier integrity and permeability. *Journal of drug targeting* **12**, 635-641 (2004).
80 Hare, D., Ayton, S., Bush, A. & Lei, P. A delicate balance: Iron metabolism and diseases of the brain. *Frontiers in Aging Neuroscience* **5**, doi:10.3389/fnagi.2013.00034 (2013).
81 Daniels, T. R. *et al.* The transferrin receptor and the targeted delivery of therapeutic agents against cancer. *Biochim Biophys Acta* **1820**, 291-317, doi:10.1016/j.bbagen.2011.07.016 (2012).
82 Luck, A. N. & Mason, A. B. Transferrin-mediated cellular iron delivery. *Curr Top Membr* **69**, 3-35, doi:10.1016/b978-0-12-394390-3.00001-x (2012).
83 Tortorella, S. & Karagiannis, T. C. Transferrin receptor-mediated endocytosis: a useful target for cancer therapy. *J Membr Biol* **247**, 291-307, doi:10.1007/s00232-014-9637-0 (2014).
84 Luck, A. N. & Mason, A. B. Structure and dynamics of drug carriers and their interaction with cellular receptors: focus on serum transferrin. *Advanced drug delivery reviews* **65**, 1012-1019, doi:10.1016/j.addr.2012.11.001 (2013).
85 Aisen, P., Leibman, A. & Zweier, J. Stoichiometric and site characteristics of the binding of iron to human transferrin. *J Biol Chem* **253**, 1930-1937 (1978).
86 Moos, T. & Morgan, E. H. Transferrin and transferrin receptor function in brain barrier systems. *Cell Mol Neurobiol* **20**, 77-95, doi:10.1023/a:1006948027674 (2000).
87 Cheng, Y., Zak, O., Aisen, P., Harrison, S. C. & Walz, T. Structure of the human transferrin receptor-transferrin complex. *Cell* **116**, 565-576, doi:10.1016/s0092-8674(04)00130-8 (2004).
88 Khan, A. I., Liu, J. & Dutta, P. Iron transport kinetics through blood-brain barrier endothelial cells. *Biochimica et Biophysica Acta (BBA) - General Subjects* **1862**, 1168-1179, doi:https://doi.org/10.1016/j.bbagen.2018.02.010 (2018).
89 Pearse, B. M. & Robinson, M. S. Clathrin, adaptors, and sorting. *Annual review of cell biology* **6**, 151-171 (1990).

90 Roberts, R. L., Fine, R. E. & Sandra, A. Receptor-mediated endocytosis of transferrin at the blood-brain barrier. *J Cell Sci* **104 (Pt 2)**, 521-532 (1993).
91 Chiou, B. *et al.* Endothelial cells are critical regulators of iron transport in a model of the human blood-brain barrier. *J Cereb Blood Flow Metab* **39**, 2117-2131, doi:10.1177/0271678x18783372 (2019).
92 Burkhart, A. *et al.* Expression of Iron-Related Proteins at the Neurovascular Unit Supports Reduction and Reoxidation of Iron for Transport Through the Blood-Brain Barrier. *Mol Neurobiol* **53**, 7237-7253, doi:10.1007/s12035-015-9582-7 (2016).
93 Simpson, I. A. *et al.* A novel model for brain iron uptake: introducing the concept of regulation. *J Cereb Blood Flow Metab* **35**, 48-57, doi:10.1038/jcbfm.2014.168 (2015).
94 Chiou, B. *et al.* Endothelial cells are critical regulators of iron transport in a model of the human blood–brain barrier. *Journal of Cerebral Blood Flow & Metabolism* **39**, 2117-2131, doi:10.1177/0271678x18783372 (2019).
95 Aldred, A. R., Dickson, P. W., Marley, P. & Schreiber, G. Distribution of transferrin synthesis in brain and other tissues in the rat. *Journal of Biological Chemistry* **262**, 5293-5297 (1987).
96 Moos, T., Rosengren Nielsen, T., Skjorringe, T. & Morgan, E. H. Iron trafficking inside the brain. *J Neurochem* **103**, 1730-1740, doi:10.1111/j.1471-4159.2007.04976.x (2007).
97 Skjorringe, T., Burkhart, A., Johnsen, K. B. & Moos, T. Divalent metal transporter 1 (DMT1) in the brain: implications for a role in iron transport at the blood-brain barrier, and neuronal and glial pathology. *Front Mol Neurosci* **8**, 19, doi:10.3389/fnmol.2015.00019 (2015).
98 Johnsen, K. B., Burkhart, A., Thomsen, L. B., Andresen, T. L. & Moos, T. Targeting the transferrin receptor for brain drug delivery. *Progress in Neurobiology* **181**, 101665, doi:https://doi.org/10.1016/j.pneurobio.2019.101665 (2019).
99 Laske, D. W., Youle, R. J. & Oldfield, E. H. Tumor regression with regional distribution of the targeted toxin TF-CRM107 in patients with malignant brain tumors. *Nat Med* **3**, 1362-1368, doi:10.1038/nm1297-1362 (1997).
100 Weaver, M. & Laske, D. W. Transferrin Receptor Ligand-Targeted Toxin Conjugate (Tf-CRM107) for Therapy of Malignant Gliomas. *Journal of Neuro-Oncology* **65**, 3-14, doi:10.1023/A:1026246500788 (2003).
101 Lichota, J., Skjorringe, T., Thomsen, L. B. & Moos, T. Macromolecular drug transport into the brain using targeted therapy. *J Neurochem* **113**, 1-13, doi:10.1111/j.1471-4159.2009.06544.x (2010).
102 Fullstone, G., Nyberg, S., Tian, X. & Battaglia, G. in *International Review of Neurobiology* Vol. 130 (ed Khuloud T. Al-Jamal) 41-72 (Academic Press, 2016).
103 Alam, K. K., Chang, J. L. & Burke, D. H. FASTAptamer: A Bioinformatic Toolkit for High-throughput Sequence Analysis of Combinatorial Selections. *Mol Ther Nucleic Acids* **4**, e230, doi:10.1038/mtna.2015.4 (2015).
104 Wang, X., Lim, H. J. & Son, A. Characterization of denaturation and renaturation of DNA for DNA hybridization. *Environmental health and toxicology* **29** (2014).
105 Musheev, M. U. & Krylov, S. N. Selection of aptamers by systematic evolution of ligands by exponential enrichment: addressing the polymerase chain reaction issue. *Analytica chimica acta* **564**, 91-96 (2006).
106 Polz, M. F. & Cavanaugh, C. M. Bias in template-to-product ratios in multitemplate PCR. *Appl. Environ. Microbiol.* **64**, 3724-3730 (1998).

107 Levay, A. *et al.* Identifying high-affinity aptamer ligands with defined cross-reactivity using high-throughput guided systematic evolution of ligands by exponential enrichment. *Nucleic Acids Res* **43**, e82, doi:10.1093/nar/gkv534 (2015).
108 Chen, C., Zhou, S., Cai, Y. & Tang, F. Nucleic acid aptamer application in diagnosis and therapy of colorectal cancer based on cell-SELEX technology. *NPJ precision oncology* **1**, 1-7 (2017).
109 Huang, H.-L. *et al.* Trypsin-induced proteome alteration during cell subculture in mammalian cells. *Journal of biomedical science* **17**, 36 (2010).
110 Gatter, K. C., Brown, G., Trowbridge, I., Woolston, R. & Mason, D. Transferrin receptors in human tissues: their distribution and possible clinical relevance. *Journal of clinical pathology* **36**, 539-545 (1983).
111 Prost, A. C. *et al.* Differential transferrin receptor density in human colorectal cancer: A potential probe for diagnosis and therapy. *Int J Oncol* **13**, 871-875, doi:10.3892/ijo.13.4.871 (1998).
112 Shindelman, J. E., Ortmeyer, A. E. & Sussman, H. H. Demonstration of the transferrin receptor in human breast cancer tissue. Potential marker for identifying dividing cells. *Int J Cancer* **27**, 329-334, doi:10.1002/ijc.2910270311 (1981).
113 Larrick, J. W. & Cresswell, P. Modulation of cell surface iron transferrin receptors by cellular density and state of activation. *Journal of supramolecular structure* **11**, 579-586 (1979).
114 Jefferies, W. A. *et al.* Transferrin receptor on endothelium of brain capillaries. *Nature* **312**, 162-163, doi:10.1038/312162a0 (1984).
115 Pardridge, W. M. Blood-brain barrier drug delivery of IgG fusion proteins with a transferrin receptor monoclonal antibody. *Expert Opin Drug Deliv* **12**, 207-222, doi:10.1517/17425247.2014.952627 (2015).
116 Xia, C.-F., Zhang, Y., Zhang, Y., Boado, R. J. & Pardridge, W. M. Intravenous siRNA of Brain Cancer with Receptor Targeting and Avidin–Biotin Technology. *Pharmaceutical Research* **24**, 2309-2316, doi:10.1007/s11095-007-9460-8 (2007).
117 Yu, Y. J. *et al.* Therapeutic bispecific antibodies cross the blood-brain barrier in nonhuman primates. *Sci Transl Med* **6**, 261ra154, doi:10.1126/scitranslmed.3009835 (2014).
118 Ohashi, P. S. *et al.* Reconstitution of an active surface T3/T-cell antigen receptor by DNA transfer. *Nature* **316**, 606-609, doi:10.1038/316606a0 (1985).
119 Zadeh, J. N. *et al.* NUPACK: analysis and design of nucleic acid systems. *Journal of computational chemistry* **32**, 170-173 (2011).
120 Wu, X. *et al.* Elucidation and structural modeling of CD71 as a molecular target for cell-specific aptamer binding. *Journal of the American Chemical Society* **141**, 10760-10769 (2019).
121 Wu, X. *et al.* DNA aptamer selected against pancreatic ductal adenocarcinoma for in vivo imaging and clinical tissue recognition. *Theranostics* **5**, 985 (2015).
122 Zuker, M. Mfold web server for nucleic acid folding and hybridization prediction. *Nucleic Acids Res* **31**, 3406-3415, doi:10.1093/nar/gkg595 (2003).
123 Biesiada, M., Purzycka, K. J., Szachniuk, M., Blazewicz, J. & Adamiak, R. W. Automated RNA 3D Structure Prediction with RNAComposer. *Methods Mol Biol* **1490**, 199-215, doi:10.1007/978-1-4939-6433-8_13 (2016).
124 Case, D. *et al.* AMBER 2018; 2018. *University of California, San Francisco*.

125 Curtis, C. D. & Nardulli, A. M. in *The nuclear receptor superfamily* 187-204 (Springer, 2009).
126 Moos, T. & Morgan, E. H. Restricted transport of anti-transferrin receptor antibody (OX26) through the blood-brain barrier in the rat. *J Neurochem* **79**, 119-129, doi:10.1046/j.1471-4159.2001.00541.x (2001).
127 Altschul, S. F., Gish, W., Miller, W., Myers, E. W. & Lipman, D. J. Basic local alignment search tool. *Journal of molecular biology* **215**, 403-410 (1990).
128 Lesley, J. F. & Schulte, R. J. Inhibition of cell growth by monoclonal anti-transferrin receptor antibodies. *Mol Cell Biol* **5**, 1814-1821, doi:10.1128/mcb.5.8.1814 (1985).
129 Daniels, T. R., Delgado, T., Rodriguez, J. A., Helguera, G. & Penichet, M. L. The transferrin receptor part I: Biology and targeting with cytotoxic antibodies for the treatment of cancer. *Clinical immunology* **121**, 144-158 (2006).
130 Neiveyans, M. *et al.* A recycling anti-transferrin receptor-1 monoclonal antibody as an efficient therapy for erythroleukemia through target up-regulation and antibody-dependent cytotoxic effector functions. *MAbs* **11**, 593-605, doi:10.1080/19420862.2018.1564510 (2019).
131 Jørgensen, A. S., Hansen, L. H., Vester, B. & Wengel, J. Improvement of a streptavidin-binding aptamer by LNA-and α-l-LNA-substitutions. *Bioorganic & medicinal chemistry letters* **24**, 2273-2277 (2014).